PREPARATION OF DENSE BARIUM CERATE FILM ON A PLANAR POROUS SUPPORT FOR HYDROGEN SEPARATION MEMBRANES

By

RUCHITA D. BAGUL

A THESIS PRESENTED TO THE GRADUATE SCHOOL
OF THE UNIVERSITY OF FLORIDA IN PARTIAL FULFILLMENT
OF THE REQUIREMENTS FOR THE DEGREE OF
MASTER OF SCIENCE

UNIVERSITY OF FLORIDA

2004

ACKNOWLEDGMENTS

I would like to thank Dr Eric Wachsman for giving me an opportunity to work under his guidance. I would also like to thank Dr Daryl Butt and Dr Wolfgang Sigmund for being on my committee. Also thanks go to Keith, Dr Hee-Sung Yoon, Sun-Ju, Jun, Abhishek, Guojing, Matt, Jamie, Briggs and all others for helping me in my project.

Above all I thank my parents and my brother who supported me during all this time and helped me overcome my problems.

TABLE OF CONTENTS

page

ACKNOWLEDGMENTS iii

LIST OF TABLES vi

LIST OF FIGURES vii

ABSTRACT ix

CHAPTER

1 LITERATURE REVIEW 1

Introduction 1
Ceramic Membranes and Protonic Conductivity 3
Why a Thin Dense Ceramic Film Required? 5
Classification Of Proton Conductors 7
High Temperature Proton Conducting Oxides(HTPC) 7
Intermediate Temperature Proton Conductors 7
Low Temperature Proton Conducting Polymers 8
Transport Process 10
Proton Migration methods 10
Proton Conduction 11
Proton Diffusion 14
Stability of Perovskite Oxides 15
Processing of Ceramics 19
Pechini Process 20
Homogeneous Oxalate Coprecipitation 20
Glycine Nitrate Process 21
Porbaix Diagram 21
Film Deposition 24
Colloidal Deposition 26
Spin Coating 27
Tape Casting 28

2 PREPARATION OF DENSE BARIUM CERATE FILM ON A PLANAR POROUS SUPPORT FOR HYDROGEN SEPARATION MEMBRANE 30

Experimental 30

Preparation of Barium Cerate Electrolyte Powders....30
Results and Discussions....33
Characterization....33
TGA-DTA Results....33
XRD Observations....36
Particle Size distribution....41
Determination of optimum sintering temperature and microstructure of film....41
Conclusions....42

3 PREPARATION OF DENSE EUROPIUM DOPED BARIUM-CERATE FILM ON A PLANAR POROUS SUPPORT FOR HYDROGEN SEPARATION MEMBRANE....47

Experimental....48
Preparation of Eu Doped Barium Cerate Powder....48
Slurry preparation and Spin coating....49
Results and Discussions....50
Conclusions....51
CONCLUSIONS....66

LIST OF REFERENCES....71

BIOGRAPHICAL SKETCH....77

LIST OF TABLES

Table page

1 Possible devices using HTPC solid electrolytes 9

2 Composition of slurry for spin coating 49

LIST OF FIGURES

Figure page

1. Structure of a perovskite structure of type ABO_3 (A=Ba, B=Ce in $BaCeO_3$).....4

2. Schematical use of mixed oxygen ion–electronic conductor for oxygen 6

3. The trace of a proton in a perovskite showing two principal features 17

4. Effect of orthorhombic distortion of $BaCeO_3$ and $SrCeO_3$ on the basicity of O_1 18

5. Porbaix diagrams for barium , cerium and europium metal 25

6. Schematic of a Tape Casting Machine.....29

7. Proton conductivities of various oxides as calculated from data on proton 32

8. TGA-DTA measurements of powders from Pechini process 34

9. XRD spectra for powders made by Pechini process 37

10. XRD spectra according to content of citric acid 38

11. XRD spectra for powder calcined at 1100 ^oC by Oxalate method 39

12. Particle size distribution for powder calcined at 1100 ^oC from oxalate method. 39

13. Particle size distribution for Pechini powder calcined at 1000 ^oC 40

14. Shrinkage rate % vs Temperature between $BaCeO_3$ and NiO-GDC powder 43

15. Surface view of film from oxalate powder sintered at 1300 ^oC.....44

16. Surface view of film from oxalate powder sintered at 1400 ^oC.....44

17. Surface view of film from oxalate powder sintered at 1500 ^oC.....45

18. Cross-section view of film from oxalate powder sintered at 1500 ^oC 45

19. Surface view of film from Pechini powder sintered at 1500 ^oC 46

20. Cross-section view of film from Pechini powder sintered at 1500 ^oC.....46

21. Flow chart for preparation of Tape Cast substrate. 53

22. Surface view of spin coated film sintered at 1400 ^{o}C on tape cast substrate 54

23. Surface view of spin coated film sintered at 1450 ^{o}C on tape cast substrate 55

24. Surface view of spin coated film sintered at 1500 ^{o}C on tape cast substrate 56

25. Cross-section view of spin coated film sintered at 1500 ^{o}C on tape cast substrate 57

26. Surface view of spin coated film sintered at 1400 ^{o}C on tape cast substrate 58

27. Surface view of spin coated film sintered at 1500 ^{o}C on Uniaxially 59

28. Cross-section view of spin coated film sintered at 1500 ^{o}C on Uniaxially 60

29. Surface view of spin coated film sintered at 1500 ^{o}C on tape cast 61

30. Surface view of spin coated film sintered at 1500 ^{o}C on tape cast substrate 62

31. Cross-section view of spin coated film sintered at 1500 ^{o}C on tape cast substrate 63

32. Film sintered at 1500 ^{o}C.for 5hours 64

33. Film sintered at 1500 ^{o}C for 8 hours. 64

34. Film sintered at 1600 ^{o}C for 5 hours 65

35. Film sintered at 1600 ^{o}C for 8 hours. 65

Abstract of Thesis Presented to the Graduate School
of the University of Florida in Partial Fulfillment of the
Requirements for the Degree of Master of Science

PREPARATION OF DENSE BARIUM CERATE FILM ON A PLANAR POROUS SUPPORT FOR HYDROGEN SEPARATION MEMBRANES

By

Ruchita D. Bagul

August 2004

Chair: Eric Wachsman
Major Department: Materials Science and Engineering

Perovskite based compounds are being researched for their high proton conductivities. Of the different perovskite materials available, barium cerate is widely being studied as a potential material for hydrogen separation membranes. It has been shown to exhibit high protonic conductivities at high temperatures in the presence of watervapour or hydrogen atmosphere.

In the first phase barium cerate was prepared by the Pechini and Oxalate Co-precipitation method, and the powder obtained was calcined at high temperatures. The powder was characterized by XRD for determination of single phase and BET Coulter for particle size. Nickel oxide-gadolinium doped ceria substrate was prepared by uniaxial press method and barium cerate film was deposited by dip coating. The film was fired at different temperatures to obtain a dense film. Scanning Electron Microscopy was done to

determine the film density. Sintering temperature of 1500 ^{o}C was found to give a dense film though the film still exhibited some porosity.

In the second phase europium doped barium cerate was made by the oxalate method while the substrate was made by the tape casting method. Films were deposited on uniaxially pressed and tape casted substrates by spin coating. Films on tape casted substrate were more dense than those on the uniaxial pressed ones. Dense patches of film with some pores were found which could be due to the difference in shrinkage rates between the film and substrate material.

CHAPTER 1
LITERATURE REVIEW

Introduction

According to scientists hydrogen is believed to be formed during a "Big Bang" some 15 million years ago. Discovered by an English chemist Henry Cavendish some 200 years ago (1), hydrogen is being looked at as a potential source for fulfilling the worlds energy needs in the 21st century. Nations all over the world are trying to find ways to harness this readily available energy so that it can be put to use.

So why is the entire world suddenly trying to move to a hydrogen economy? Let us first have a brief overview of hydrogen first. The world hydrogen comes from the Greek words "hydro" (meaning water) and "genes" (meaning generator) (1). It is the simplest, lightest and most abundant element in the universe. And now it has been found that hydrogen as a fuel could be the best alternative to replace the depleting natural energy reserves.

To list a few advantages of using hydrogen as a fuel:

- It is an excellent energy carrier.
- No green house gases are generated in its use since there is no carbon in the fuel.
- Hydrogen can reduce the depletion of fossil fuel reserves.
- Hydrogen holds more chemical energy pound for pound than any other fuel.
- Hydrogen produces effectively zero emissions when it is burned in an engine and only water when powering a fuel cell.
- It can be produced from the abundantly available domestic resources such as natural gas, coal, biomass and even water.

A look at the American oil requirement shows that America imports 55% of the oil it consumes which is expected to grow to 68% by 2025 (2). Hydrogen economy could reduce this dependence by over 11 million barrels per day by 2040. This in turn could reduce the greenhouse gas emissions from transportation alone by more than 500 million metric tons of carbon equivalent each year by 2040 (2). Considering these socioeconomic and environmental advantages which are also applicable more or less to the rest of the world there is a huge incentive in trying to develop cost effective ways of producing hydrogen.

There are a variety of ways by which hydrogen can be extracted from different sources:

- Steam reforming of methane to produce hydrogen and carbon monoxide by reaction with steam over a nickel catalyst.
- Electrolysis to split water into hydrogen at cathode and oxygen at anode.
- Themochemical water splitting using chemicals and heat.
- Biological systems in which microbes break down biomass into hydrogen.
- Thermal water splitting using high temperatures.
- Photoelectrochemical systems use semiconducting materials to split water using sunlight.

For the next few decades, hydrogen will be generated from fossil fuels until cleaner hydrogen sources can be developed. Pure H_2 streams will need to be produced via separation from mixed gas streams containing CO, CO_2, H_2O, hydrocarbons and other gases by separation processes. Pure H_2 is needed for fuel cells, to facilitate H_2 storage, to recover H_2 from mixed gas products in the petrochemical industries, and for upgrading of petroleum products to fuels (3). However at present there are no viable high temperature separation membranes capable of producing pure H_2 streams. This area of research needs

to be rapidly expanded over the next decade if the Hydrogen Economy is to become a reality.

Ceramic Membranes and Protonic Conductivity

Ion transport membranes composed of proton conducting materials are a critical component for future fuel processing and energy production systems, as well as ancillary technologies such as fuel cells, sensors, and electrolyzers. Proton conducting membranes are necessary to extract pure hydrogen from mixed gas streams in the processing of fossil fuels and other petroleum and petrochemical processes. The best candidate membrane materials for hydrogen separation at high temperatures are proton conducting ceramic oxides.

In the 1980's Iwahara et al. discovered that perovskite based oxides had the ability of high temperature proton conduction. $SrCeO_3$ and BaCeO3 doped with trivalent cations such as Y, Yb, Gd and Eu have been identified as good high temperature proton conductors (4,5-10). The general formula for representing these materials is ABO_3, Figure 1 or for doped perovskites $A_{1-x}A_xB_{1-y}B_yO_{3-\delta}$, where x and y are the fraction of dopants in the A and B site respectively and δ is the number of oxygen vacancies. Oxygen vacancies can be produced by doping the B site with lower valence cations. Different parameters such as dopant concentration, the number of oxygen vacancies, atmospheric conditions and temperature etc. determine the quantity of proton charge carriers that can be introduced in a given material. In case of BaCeO3 depending on the exact composition and operation conditions proton concentrations varying from 0.1 mole% to greater than 10 mole% can be obtained (5,11-14). Doping these perovskite materials increases the charge carrier concentration which in turn increases the proton conductivity when compared with the undoped materials.

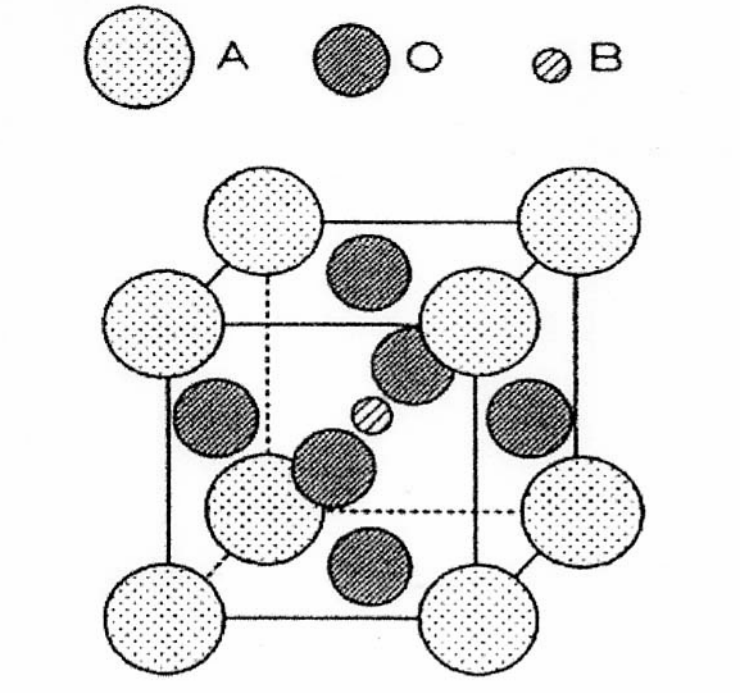

Figure 1. Structure of a perovskite structure of type ABO_3 (A=Ba, B=Ce in $BaCeO_3$)

Hydrogen separation can be achieved using a dense ceramic based membrane. Figure 2 shows how pure hydrogen can be extracted from a mixture of gases. Here a syngas mixture (H_2, CO and CO_2) is passed across the membrane surface where catalytic oxidation of hydrogen takes place. Protons and electrons are generated which incorporate into the material membrane lattice, which are then conducted to the reduction surface. A reverse reduction reaction occurs at this surface and pure hydrogen is produced. If this technology is able to produce reasonable separation rates it can offer following advantages over alternative separation methods (15):

- The membrane materials are relatively inexpensive and the system design is inherently simple.
- The membrane is nonporous, therefore only hydrogen is transported without other gases leaking through.
- As a result purification steps are not required and membranes are not subject to problems associated with pore clogging.
- The transport method in this materials occurs at temperatures compatible with incorporation into chemical processing streams.
- Being highly versatile the membrane system can be used to facilitate numerous chemical processing applications by appropriately adjusting the catalyst.

Why a Thin Dense Ceramic Film Required?

There are a number of advantages in fabricating thin film ceramic membranes. Ohmic losses across ionic and mixed ionic-electronic conducting materials are reduced as membrane thickness is reduced. When films are very thin the resistance of the electrolyte at intermediate temperatures is almost negligible (16). As a result the electrochemical device can operate at lower temperatures and higher thermodynamic efficiency. Thin films also enhance surface exchange kinetics and diffusion phenomenon. The technical challenge involves depositing pinhole and crack free dense layers of membrane 5 to 40

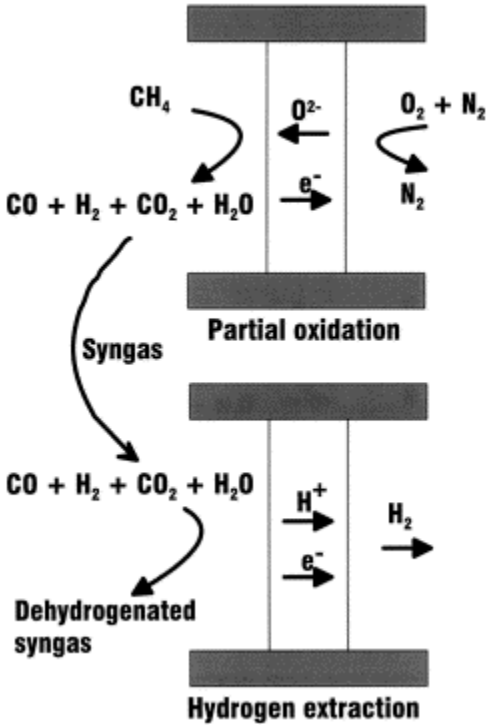

Figure 2. Schematical use of mixed oxygen ion–electronic conductor for oxygen separation with direct partial oxidation of methane, followed by use of mixed protonic–electronic conductor for hydrogen extraction.(From T. Norby, Solid State Ionics, 136 (2000) 139)

μm in thickness on substrates of high porosity. The film must be well bonded to the substrate without excessive infilteration into the electrode porosity and there must be minimal interface polarization (16).

Classification Of Proton Conductors

High Temperature Proton Conducting Oxides(HTPC)

Stotz and Wagner first investigated proton transport (17) after proton conductivity was first reported in 1960's (18). Cerates were reported to have highest proton conductivity as reported by Iwahara et al (19). The perovskite type oxides exhibit p-type electronic conductivity at high temperatures in absence of hydrogen or water-vapour. But when exposed to elevated temperature in presence of hydrogen or reducing atmosphere, protonic conduction appears with decrease in electronic conductivity. The conductivities are of the order of 10^{-2} to 10^{-3} Scm^{-1} at 600-1000 ^{o}C (20,21). Among the cerate oxides $SrCeO_3$ and $BaCeO_3$ exhibit the most protonic conductivity.

Proton conducting ceramics have two fundamental functions that can be used for protonic devices. They are functions of electromotive force and electrochemical hydrogen transport in solids (22). Possible devices using HTPC solid electrolytes are listed in Table 1 classified according to the above functions .

Intermediate Temperature Proton Conductors

Very few materials show proton conductivity at intermediate temperatures (100-400 ^{o}C). Heterocycles such as imidazole exhibits moderate proton conductivity at these temperatures. The nitrogen group acts as a strong proton acceptor w.r.t. Bronsted acids such as sulphonic acid groups forming protonic charge carriers $(C_3H_3NH_2)^+$ (34).The protonated and unprotonated nitrogen groups in the nonpolar ring may act as donors and acceptors in proton transfer reactions (5). The high melting point of these materials

supports proton conductivity at moderate temperature while chemical compatibility with other compounds is due to its high basicity.

Low Temperature Proton Conducting Polymers

Polymer electrolyte membrane fuel cells (PEM-FC) have been used for a long time in space crafts and submarines. Perfluorinated ion exchange membranes in their protonic form such as NAFION are used as membrane material.

Nafion's extremly hydrophobic perfluorinated polymer backbone provides good mechanical stability in presence of water, while the sulphonic acid group is highly hydrophilic and provides a very high proton conductivity due to high mobility of water molecules that act as proton vehicles (23).

In the presence of water a stationary microstructure is formed which absorbs and deabsorbs at moderate temperatures. The activation enthalpy for water diffusion in such membranes is almost equal to that in pure water, while the absolute value of diffusion coefficients decreases with decreasing water content (24).

Other sulphonated membrane materials are sulphonated styrene grafted FEP (25), sulphonated ORMOCERs (26), partially fluorinated polystyrenes (27) and organically modified layered phosphonates (28). Ryton and PEK (29) can be developed as chemically durable proton conducting polymers (30,31). These allow for direct electrophilic sulphonation which is inexpensive compared to fabrication of perfluorosulphonic membranes. Comparing the properties of Nafion with these new membranes shows that nanoseperation (32) has positive effects on proton and water diffusion and morphological stability and it could provide an interesting route for silmultaneously improving membrane properties for fuel cell applications (33).

Table 1: Possible devices using HTPC solid electrolytes

Function	Phenomena applicable	Devices
EMF	Signal	Hydrogen gas sensor Steam sensor Hydrocarbon sensor
	Power	Fuel cells
Electrochemical permeation of hydrogen	Seperation	Hydrogen extractor Steam pump Isotope concentrator
	Electrolysis	H2S electrolyser for desulphurization HCl electrolyser for Cl2 recovery Steam electrolyser for H2 production
	Reaction	Membrane reactors for hydrogenation and dehydrogenation of organic compounds

From H. Iwahara, Solid State Ionics 3-4, (2003) 164.

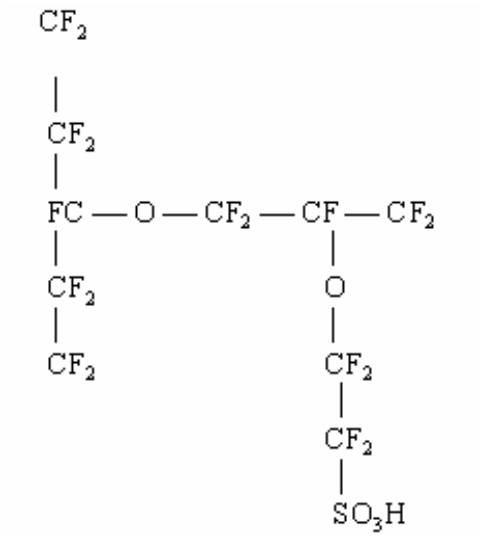

Structure of Nafion
(From F. M. Krug, Doctoral Thesis, RWTH Aachen (1996)

Transport Process

Proton Migration methods

There are two ways of proton migration in oxides: Free migration and Vehicle mechanism. In the free migration mechanism, the proton moves by jumping between stationary host oxygen ions while the vehicle mechanism involves movement of proton as a passenger on a larger ion like OH^- or H_3O^+ (13). Free proton migration is a dominating mechanism in oxides at high temperature. Isotope effects assume a large importance in free migration of hydrogen than any other diffusion process due to the unique 1:2:3 mass ratios of protium (H), deuterium (D) and tritium (T) isotopes of hydrogen. Three effects are mainly recognized (34)

1. The "classical" difference: The preexponential of diffusion is inversely proportional to the square root of the mass of hydrogen isotope; $D_H:D_D:D_T = 1:(1/\sqrt{2}):(\sqrt{3})$. Since these ratios are easy to detect they are used to distinguish between free hydrogen migration and vehicle mechanism.

2. The "nonclassical" difference;Hydrogen isotopes have different masses and so different zero-point energy levels due to which there is a difference in activation energy for diffusion.

3. Tunneling; Hydrogen diffusion is enhanced due to the tunneling effect made possible by light protons.

Proton Conduction

The introduction of protons into the perovskite ceramic is usually shown in terms of moisture containing gas streams as an acid/base equilibrium between water molecules and oxygen vacancies. Using Kroger-Vink notation (35) oxygen vacancies, $V_o^{\cdot\cdot}$, react with water to fill lattice positions with oxide ions, O_o^x, and produce interstitial protons, $H_i^{\cdot}$, according to (5),

$$H_2O + V_o^{\cdot\cdot} \leftrightarrow O_o^x + 2H_i^{\cdot} \quad (1)$$

Protons are retained in the material by associating with oxide ions at normal lattice sites,

$$O_o^x + H_i^{\cdot} = OH_o^{\cdot} \quad (2)$$

So that the net reaction demonstrating the interaction of oxygen vacancies with water-vapour to produce proton charge carriers can be written as,

$$H_2O + V_o^{\cdot\cdot} + O_o^x \leftrightarrow 2OH_o^{\cdot} . \quad (3)$$

But hydrogen in the gas stream is incorporated directly into the material as protons and electrons (e') through interaction with oxide ions in the absence of moisture according to,

$$1/2H_2 + O_o^x \leftrightarrow OH_o^{\cdot} + e' . \quad (4)$$

Processes occurring at opposite surfaces of the membranes cause conduction of protons and electrons across the ceramic membrane. The ratio of hydrogen partial pressure on opposite sides of the membrane in case of hydrogen separation, causes a concentration gradient corresponding to a Nernstian potential difference. This potential difference determines the rate of conduction up to the catalysis, mass transfer or material limited rate (15).

It has been argued that protons are conducted not only by transference between oxygen ions at normal lattice site positions but also by OH^- conduction as well (5,11,13,35). A number of techniques have been used to determine the dominant charge carrier in perovskite materials, and the conclusion of proton "hopping" at moderate temperatures (less than 800^oC) is based on

- Isotope effect studies that demonstrate the predicted √2factor greater conductivity for protons than deuterium ions (7,36)
- Chemical analysis of the product effluents from electrochemical cells under DC conditions (4,36-38).
- Comparision of measured and theoretical potentials from hydrogen and steam concentration cells (6,39,40)
- O diffusivity experiments that largely rule out OH^- transport (35,36)

As oxygen ions move closer during a vibration, the energy barrier for proton transfer diminishes (5). Quantum molecular dynamic simulation studies of proton conduction in $BaCeO_3$, $BaTiO_3$ and $BaZrO_3$ suggested the degree of covalence between B site cations and oxygen anions, and the degree of hydrogen bonding within the lattice are responsible for conductivity (41,42). Materials with open crystal structure mean greater separation between oxygen anions and low B-O covalence which gives softer B-O vibrations, facilitating transfer of protons between oxygen sites. Corresponding to the molecular vibrations the potential barrier for proton transfer oscillates between high and low values. In case of high hydrogen bonding since protons are in contact with adjacent oxygen anions proton conduction is also said be to high. But this means more closely packed oxygen anions and stiffer B-O vibrations which limits proton conduction. So a compromise between oxygen-oxygen separation and the stiffness of the B-O bonds must be achieved to maximize proton conductivity (41,42).

The formation of protonic defects can be considered as an amphoteric reaction where the oxide acts as a base and acid as well since a water molecule is eventually split into a hydroxide ion and a proton. As Bronsted basicity of the oxide decreases the enthalpy of the hydration reaction tends to become more exothermic (43). Most negative hydration enthalpies have been reported for similar electronegativities of A- and B- site cations (44).This data has been compared for perovskites with A- site elements only. In case of B- site element, with increasing electronegativity of the B- site cation the equilibrium constant of the hydration reaction reaction decreases in the order of cerates → zirconate → niobate → titanate (45). For binary rare earth oxides vacancy on an oxide ion is filled by an oxide ion. This difference could be due to the small variation of lattice basicity in rare earth oxides and the low oxide ion formation enthalpies in perovskites as a result of low bond strengths and strong relaxation effects. (43,46,47).

The principal features of the transport mechanism are rotational diffusion of the protonic defect (Figure 3) and proton transfer towards a neighbouring oxide ion i.e. the protons show long range diffusion while the oxygens reside on their crystallographic positions. Experimental (48-50) and quantum molecular dynamic (MD) simulations (41,51,52) have shown that rotational diffusion is fast with low activation barriers suggesting that the proton transfer reaction is the rate limiting step in the perovskites. But the strong red shifted OH-stretching absorptions in the IR spectra (5) indicate strong hydrogen bond interactions, which favour fast proton transfer reactions rather than fast reorientation processes.

Comparing $SrCeO_3$ and $BaCeO_3$ it is seen that O_1 and O_2 are the most basic ions respectively (Figure 4). Assuming that protons are associated with these sites most of the

time, O_2 site in $BaCeO_3$ may lead to long range proton transport while in $SrCeO_3$ it might involve transfer between chemically different O_1 and O_2 sites. This along with the observed biasing of defect reorientation (rotational diffusion) is thought to be the reason for higher activation enthalpy and lower conductivity in $SrCeO_3$ compared to $BaCeO_3$ (53).

Proton Diffusion

The proton conductivity is proportional to the concentration of protons which depends on oxygen, water vapour partial pressure, doping and temperature while mobility and diffusivity are independent of defect concentration. Perovskite type oxides seem to have high hydrogen diffusion coefficients (5). The self diffusion coefficient for protons can be written as an Arrehenius expression (54):

$$D = D_o \exp(-\Delta H_m / RT)$$

$$= (z d^2 N \nu_o / 6) \exp(\Delta S_m / R) \exp(-\Delta H_m / RT). \qquad (55)$$

D_o is number of possible jump directions (z), jump distance (d), fraction of vacant jump destinations (N), vibration frequency (ν_o) and jump entropy (ΔS_m). ΔH_m is the activation energy for proton migration.

It can be assumed that proton jumps only in one direction (z = 1) and over a distance equal to the oxygen-oxygen seperation in the oxide, typically 3 ^oA. N = 1 for small proton concentrations. The vibration frequency, $\nu_o = 10^{14} s^{-1}$ from IR measurements while $\exp(dS_m/R)$ is taken to be around 10 (56), which gives the value of $D_o = 0.15$ cm^2/s. Real values may vary because of complex migration routes. Calculated preexponential values for proton diffusion in rutile, TiO_2 and Yb doped $SrCeO_3$ were found to be lower

by two magnitudes and so it was suggested that only a fraction of protons take part in conduction process (20,57).

When 5% of the 4+ cation was substituted by Yb^{3+} it was seen that proton conductivity decreased in the order of $BaCeO_3$, $SrCeO_3$, $BaZrO_3$, $CaHfO_3$ as a result of increase in activation energy (20). This was attributed to decreasing lattice parameter (58). Scherban et al. (57) showed that with increasing O-O separation distance for acceptor doped $KTaO_3$, $SrCeO_3$ and $BaCeO_3$ the measured activation energies decreases. This indicates that simple proton transfer between oxygen ions is not rate limiting for diffusion and more complex interactions between protons and lattice must be considered (57).

Stability of Perovskite Oxides

For the thermodynamic stability of the oxide with respect to a certain reaction, relative stabilities with respect to reaction products have to be considered. Highly basic oxides useful in formation of proton charge carriers can also react easily with acidic or amphoteric gases such as SO_3, CO_2, or H_2O to form sulphates, carbonates or hydroxides.

The reaction of a simple perovskite ABO_3 with CO_2 can be written as

$$ABO_3 + CO_2 = AO + BO_2 + CO_2 = ACO_3 + BO_2$$

The thermodynamical data for reaction of Sr and Ba cerate with CO_2 is very similar. Since BaO is more basic than SrO, the formation of $BaCO_3$ from BaO is more advantageous than $SrCeO_3$. Hence for the above reaction the B-cation determines the stability especially if the A site is occupied by alkaline earth metals. The stability increases in the order cerates $\rightarrow$ zirconates $\rightarrow$ titanates with increasing perovskite tolerance factor (59) i.e., opposite to the direction of protonic defects. Protonic defects

are better stabilized in $BaCeO_3$ than in $SrCeO_3$, which has stronger orthorhombic distortion (10).The acceptor dopant may have some local symmetry reducing effect which is critical to the relation of the stability of the perovskite and the protonic defects.

Experiments have demonstrated that high proton conductivity and stability are antagonistic properties (5,60-62).

The formation of protonic defects and decomposition of acidic gases is favoured by oxide basicity, the stability of the oxide is anticipated to increase the formation of proton charge carriers but suppress the decomposition reaction. Independent stability tests have shown that $SrCeO_3$ and $BaCeO_3$ (a) are slightly stabilized with respect to decomposition into the binary oxide (63), (b) react to carbonates at low levels of CO_2 (64), (c) form alkaline earth hydroxides at high water activities (65).

In binary oxides if B cation is large perovskites exhibit low tolerance factor and low thermodynamic stabilization with respect to mechanical stability. The decomposition partial pressures for alkaline earth cerates are only a little higher than the corresponding alkaline earth oxides which is due to the small Gibbs free energy of formation from binary oxides. It has been claimed that barium cerate is unstable with respect to its decomposition into BaO and CeO_2 (65). Occupation of B site by Ba^{2+} in $BaCeO_3$ due to change in the grain boundary region may weaken the microstructure and lead to further destabilization (10,66). Formation of an intergrowth of Magneli and Ruddlesden-Popper phases at the surface of perovskite have been identified (67) in stable perovskites like $BaTiO_3$, $SrTiO_3$, $PbTiO_3$ etc. due to structural instabilities and is attributed to changes in oxygen partial pressure.

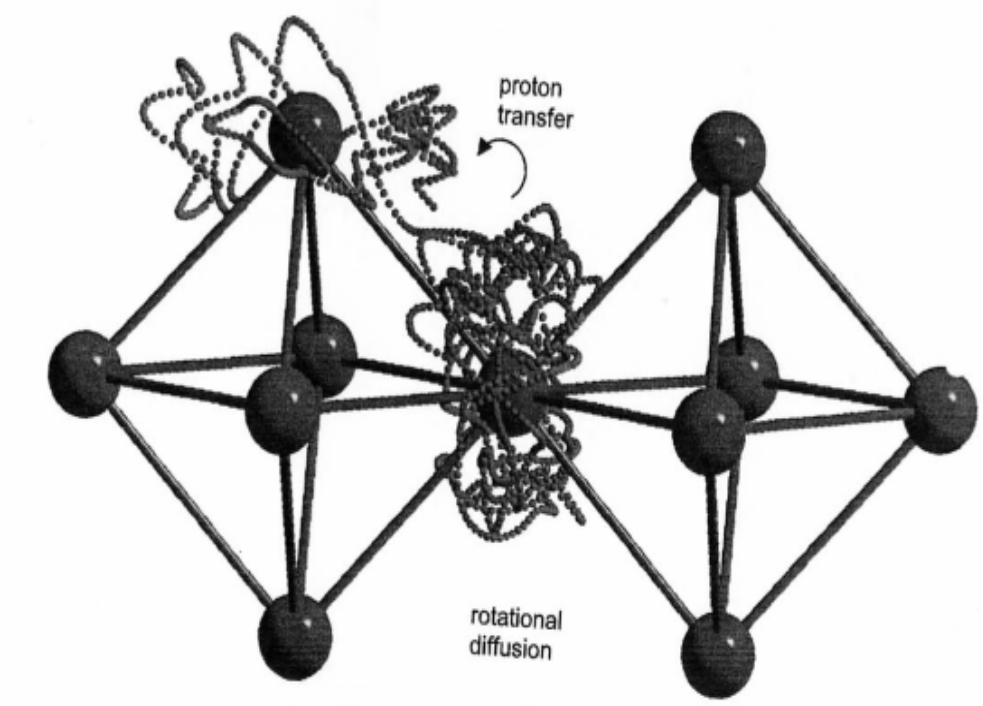

Figure 3. The trace of a proton in a perovskite showing two principal features of proton transport: rotational diffusion and proton transfer.(From K. D. Kreuer, Annu. Rev. Mater. Res., 33 (2003) 333)

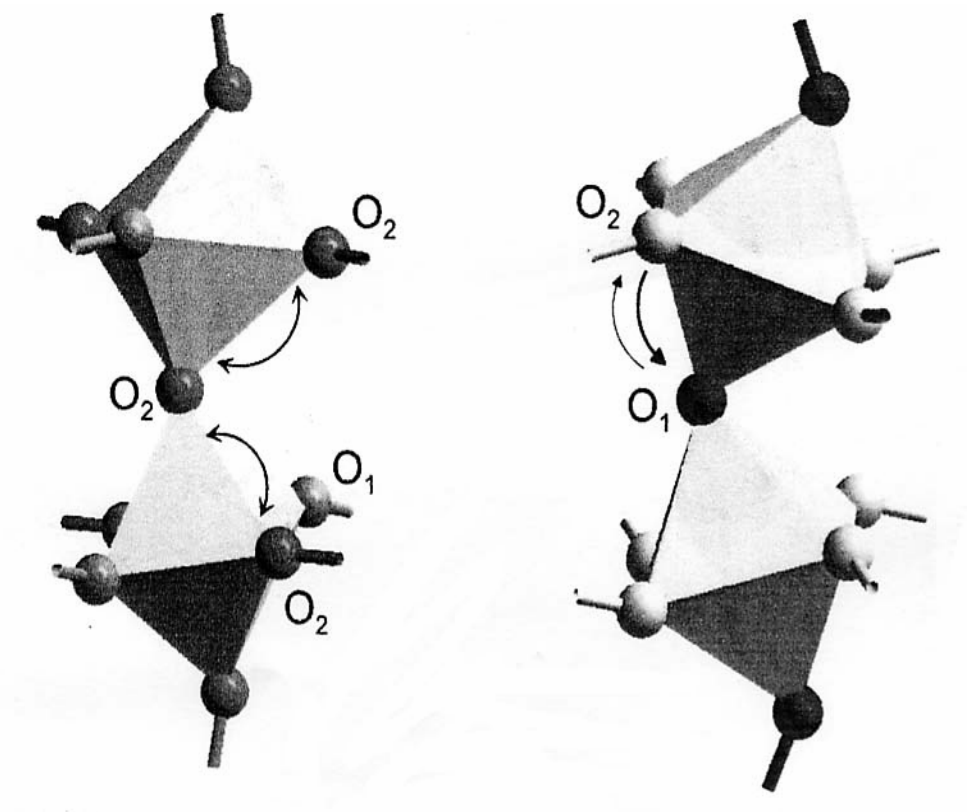

Figure 4. Effect of orthorhombic distortion of $BaCeO_3$ and $SrCeO_3$ on the basicity of O_1 and O_2 (basicity indicated by darkness of oxygen). Predominant proton transfers are indicated by arrows (From K. D. Kreuer, Annu. Rev. Mater. Res., 33 (2003) 333)

While the equilibrium constant defines upper temperature limit with respect to dehydration, for a high concentration of protonic defects, a high solubility limit is important. Loosely packed structures with less covalency exhibit high proton mobilities. Some rules for the occupation of A and B sites may help find the right perovskite for a particular application. Occupation of A-site by Ba atom gives superior results for thermodynamic stability, heat of hydration, water solubility limit and mobility of protonic defects (5). For B cation there are some restrictions. A small cation reduces the water solubility limit while a larger one results in poorer compatibility with the perovskite phase making it thermodynamically unstable so the B cation should be of medium size. The cation should be amphoteric in nature and not form any covalent bonding with the oxygen ligands. If the B cation is too basic cation it may cause decomposition reactions in acidic gases while a highly acidic cation may not generate enough negative hydration enthalpy to retain protonic defects up to the operational temperature (5). Smaller A and B cations can be used for applications where low concentration of protonic defects with high proton mobilities are desired (44,68).

Processing of Ceramics

Various ionic and mixed-conducting ceramic devices require a dense membrane and highly porous support. Dense membranes can be made by deposition of a thin film on an appropriate substrate. The ceramic powder required for making the film can be synthesized using different processes such as conventional ceramic processing, Pechini's method, modified Pechini process, homogeneous oxalate coprecipitation, electrostatic spray pyrolysis, glycine nitrate process etc.

The conventional ceramic processing involves calcining mixtures of the respective oxides, nitrates or carbonates and then sintering the powder compacts at temperatures of

1400-1600 ^{o}C (69). The solid state reaction is a diffusion controlled process which requires intimacy of reacting species and uniform distribution of each species to obtain a uniform product. The starting materials usually have a large particle size and so repeated mixing and heating at high temperatures is required so as to obtain a single phase homogeneous material (6). There is a high chance of contamination due to the abrasives used in mechanical mixing (70). The prolonged calcination process may also cause crystallite growth which is undesirable in fabrication of dense fine grained ceramics. Considering the above disadvantages powders are generally prepared using wet chemical processes such as pechini or oxalate process.

Pechini Process

In the Pechini process the desired metal cations are solvated in a solution using a hydroxycarboxylic acid, such as citric acid or ethylene diamine tetracetic acid (EDTA) as the chelating agent. EDTA is a stronger chelating agent than citric acid and is expected to improve the uniformity of metal ion distribution in the solution (71) and is used in the modified pechini method. A polyhydroxy alcohol such as ethylene glycol is then added to the solution to promote esterification reaction. Metal ions are chelated by the carboxyl groups and remain homogeneously distributed in the polymeric network (72). Further heating of the solution leads to gelation and ultimately on calcining, a powder with good compositional homogeneity and high purity is obtained. The process also requires less equipment and so is relatively inexpensive (72).

Homogeneous Oxalate Coprecipitation

In this process ammonium oxlate is added to the oxide or nitrate solution to cause precipitation of the powder. The oxalate is highly reactive and thus shortens the reaction time as well as the particle size (73). The process also imparts better homogeneity and

improved reactivity and the necessary reactions proceed rapidly at low temperatures. The addition can be done in two ways (74)

- direct strike: adding a base to an acididc cation solution
- reverse strike: adding acidic cation solution to a base

These two techniques produce very different morphologies. With the direct strike fine plately particles ~0.5 μm in size are produced while the other method produces large (> 100 μm) irregular sized particles. The difference is attributed to the degree of supersaturation in each case. Addition of base to the acidic cation solution increases the pH slowly and causes gradual precipitation while addition of acidic solution to base produces locally high supersaturation (74).

Glycine Nitrate Process

GNP is an attractive powder synthesis technique due to its potential for producing high-purity nanocrystalline powders with excellent compositional homogeneity and low energy-input requirements. Glycine is used as a fuel that can be encouraged to react with (burn) metal nitrates. A small amount of heat is required to ignite the mass if the fuel and oxidizer are intimately mixed, and if the burn is self-sustaining. In practice, however, lab scale reactions do not proceed perfectly and result in noxious gasses, fuel residue, and multi-phase product (individual metal oxides, carbonates, hydroxides, even nitrates) (75).

Porbaix Diagram

Pourbaix diagrams show the thermodynamic stability of species as a function of potential and pH. Although many basic assumptions must be considered in their derivation, such diagrams can provide valuable information in the study of corrosion phenomena. Knowledge of the pH condition of the environment is not sufficient for predicting the form in which an element will exist in natural waters. Consideration must be given to

whether the aqueous environment is well aerated (oxidizing) or polluted with organic wastes (reducing) and so the reduction potential of the environment as well as the pH have to be included in such diagram. This type of predominance diagram is known as a Pourbaix diagram.E^o-pH diagram, or pE-pH diagram (76).

Reading Porbaix diagram(77)

- Vertical lines separate species that are in acid base equilibrium.
- Non vertical lines separate species related by redox equilibria.
- Horizontal lines separate species in redox equilibria not involving hydrogen or hydroxide ions.
- Diagonal boundaries separate species in redox equilibria in which hydroxide or hydrogen ions are involved.
- Dashed lines enclose the practical region of stability of the water solvent to oxidation or reduction.

Porbain diagrams can give information about the following

- Any point on the diagram will give the thermodynamically most stable form of an element at a given potential and pH condiation.
- Strong oxidizing agents and oxidizing conditions are found at the top of Porbaix diagram while reducing agents and reducing conditions at the bottom of diagram.
- The element will undergo disproportionation when the predominance area for a given oxidation state disappears completely above or below a given pH and the element is in an intermediate oxidation state.
- A species that range from the top to the bottom of the diagram at a given pH will have no oxidizing or reducing properties at that pH.

Limitations of Porbaix diagrams

- No information on corrosion kinetics is provided.
- Diagrams are derived for specific temperature and pressure conditions.
- Diagrams are derived for selected concentrations of ionic species.
- Most diagrams consider pure substances only. Additional computations are to be made if other species are involved.
- In areas where a Porbaix diagram shows oxides to be thermodynamically stable these oxides are not necessarily of a protective nature.

Figure 1 represents the Porbaix diagram for barium, cerium and europium metal.

When the metal nitrates are dissolved in water they separate into metal ions and nitrates which then react with the oxalate to form metal oxalates But as evident from the figures the pH range and potential of each of these metals varies over which precipitation starts to occur. So it is difficult to achieve optimum precipitation. Some other compounds may also be formed in the process.

Solubility also affects the number of ions formed. Solubility product K_{sp} is equal to the product of concentration of the ions involved in the equilibrium and is constant for a given solid at a given temperature. K_{sp} influences the precipitate formation. If the ion product < K_{sp} no precipitation will occur because the molar concentration of ions is not large enough to initiate the crystallization process for precipitation to occur. If ion product > K_{sp} concentration is large enough for precipitation to occur. The concentration of ions depends on the solubility and is related to the pH. High pH suppresses solubility while a low pH will increase solubility (78).

Precipitation does not occur uniformly in a solution but proceeds through two stages called nucleation and crystal growth. Nucleation is a process of formation of tiny crystalline nuclei in the solution while crystal growth involves ordered growth of these nuclei into large well formed crystals (79). Crystal growth occurs after nuclei are formed. So larger the crystal growth, larger is the size of crystals and so larger the final particle size. If more nucleation is allowed and crystal growth is controlled it is possible to obtain particle size smaller than μm range.

Porbaix diagrams are important in case of oxalate precipitation since solubility is important in this method. Precipitation occurs in the barium cerate system hence the ionic product of the nitrates is greater than Ksp. Ammonium oxalate used in the system to cause precipitation increases the pH of the system but a balance can be obtained by adding just enough oxalate to cause precipitation and not cause a drastic increase in pH so that maximum solubility and hence more precipitation can be obtained. So the oxalate used was twice the amount of nitrates to ensure precipitation as well as enough metal ions formation. In order to maintain the complete solubility the oxalate amount can be decreased slightly but high enough to cause precipitation. The metal ions do not precipitate at the same time. As for Pechini process, precipitation is not required, the system is in the acidic medium and maxiumum solubility is obtained.

Film Deposition

There are several techniques of thin film fabrication which include vapour deposition technique (80), tape calendaring (81), sol gel deposition (72), sputtering (82), colloidal deposition (16), screen printing (83) and spin coating technique (84). High quality films can be made using some of these techniques at the expense of high equipment and operation costs while a few are relatively inexpensive.

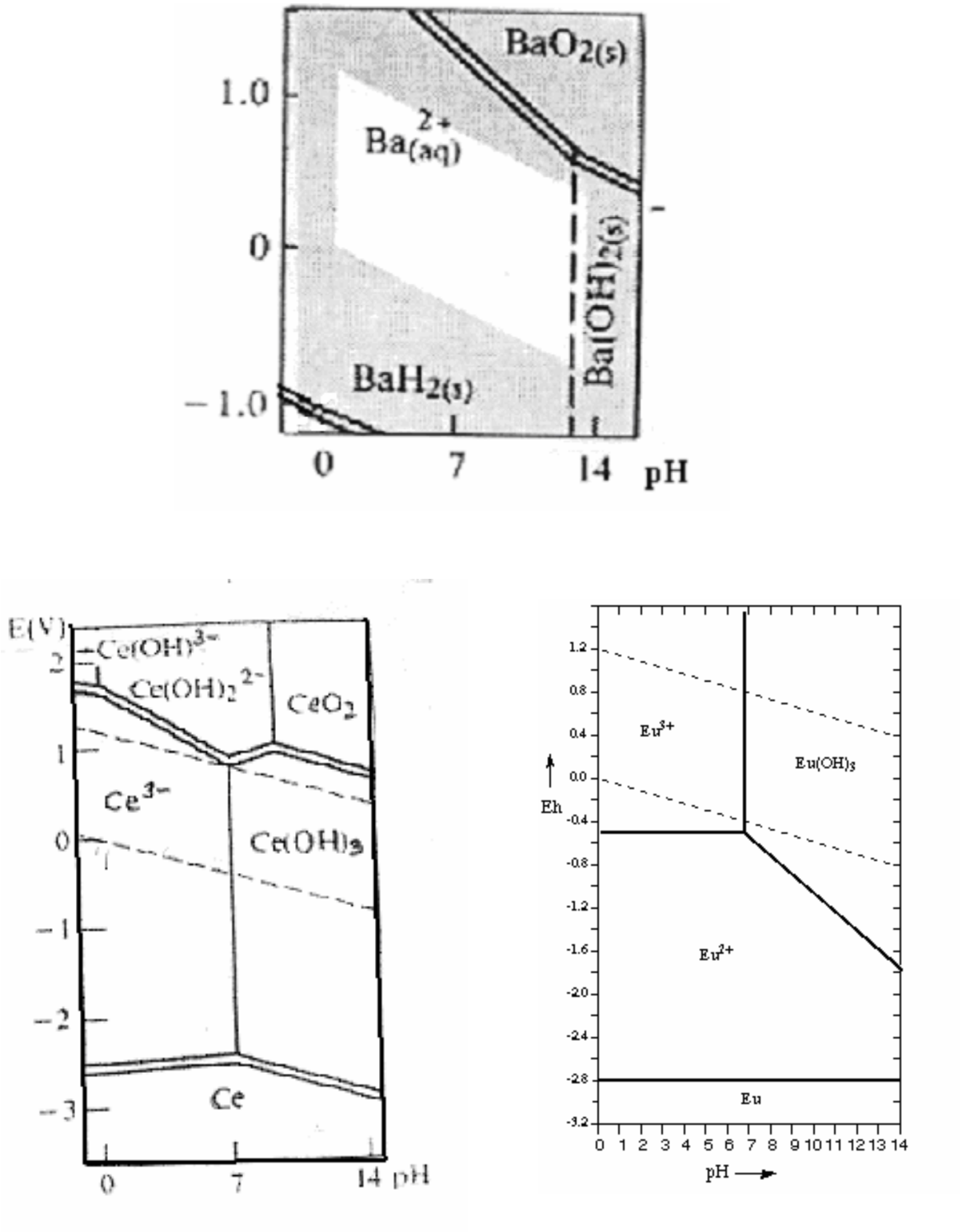

Figure 5. Porbaix diagrams for barium , cerium and europium metal (From www.wellesley.com

Colloidal Deposition

In this technique a sol is prepared by dispersing the powder in a solution which is then dipcoated on a substrate and sintered to burn off the organics and get a dense film.This technique requires that the film and substrate material are chemically compatible at the processing temperature and there should be no mismatch of thermal expansion between the layers to obtain a crack free dense film (85). The process is very flexible in that a wide variety of materials can be deposited as thin films with little to no alteration to the fabrication equipment. Also only small amount of material is needed for bilayer fabrication which makes it suitable for expensive conductors (16).

The coating thickness of the film is mainly defined by the withdrawal speed, the solid content and the viscosity of the liquid. If the withdrawal speed is chosen such that the sheer rates keep the system in the Newtonian regime, the coating thickness can be calculated by the Landau-Levich equation (86) (eq 5).

$$h = 0.94 \cdot \frac{(\eta \cdot v)^{2/3}}{\gamma_{LV}^{1/6} (\rho \cdot g)^{1/2}} \qquad (5)$$

using:

h = coating thickness

η = viscosity

γ_{LV} = liquid-vapour surface tension

ρ = density

g = gravity

Spin Coating

Spin coating is a relatively simple, low-cost approach for fabricating thin films(87). It is also an effective way to modify film thickness and microstructure(88). In the spin coating process, the substrate spins around an axis which should be perpendicular to the coating area. The spin-on process has been developed for the spin-on glasses in microelectronics and substrates with a rotational symmetry. Very homogeneous coating thickness can be obtained even with non-planer substrates. The quality of the coating depends on the rheological parameters of the coating liquid, and one should operate in the Newtonian regime. Meyerhofer (89) described the dependence of the final thickness of a spin coated layer on the processing and materials parameters like angular velocity, viscosity and solvent evaporation rate by the semi-empirical formula shown in eq. 6.

$$h = (1 - \rho_A / \rho_{Ao}) \cdot \left(\frac{3\eta \cdot m}{2\rho_{Ao} \cdot \omega^2}\right)^{1/3} \quad (6)$$

where

ρ_A =mass of volatile solvent per unit volume

ρ_{Ao} = initial value of r_A

h = final thickness

η = viscosity

ω = angular speed

m = evaporation rate of the solvent

Since m has to be determined empirically, the more simple formula, given in eq. 3 maybe used:

$$h = A \cdot \omega^{-B} \quad (90)$$

Tape Casting

This is a forming technique for producing thin, flat ceramics. The method was originally developed for producing electronic ceramics (insulating substrates and packages and multilayer capacitors). Structural laminates, knives, membranes and solid oxide fuel cells are other applications for thin ceramics formed by tape casting. The tape thickness that can be achieved is usually in the range of 25µm up to 1mm, but tapes with 5µm thickness can also be produced. Tape casting can be water based or organic solvent based system. Aqueous systems are relatively inexpensive and reduce environmental and health hazards but have disadvantages like slow drying, higher crack sensitivity, and reaction of ceramic with water in some cases. So organic based solvent systems are usually used in case of ceramics. Green tapes obtained through this method have high quality with regard to surface smoothness, flexibility and green density (91). The slurry for tape casting consists of the powder, a dispersant to stabilize the powder against colloidal forces, a solvent to reduce the mix viscosity to allow casting, a binder for green strength in the cast tape and a plasticizer to modify the properties of the binder. A powder slurry layer is formed on a carrier film by the shearing action of a doctor blade on a moving ceramic slurry. The tape is then dried. The tape contains a binder system which gives it enough 'green strength' for it to be removed from the carrier film without damage. For metal and ceramic powders the tape is then usually sintered. The binder is burnt out and the material densifies (92). A schematic of the Tape casting machine is shown in Figure 6.

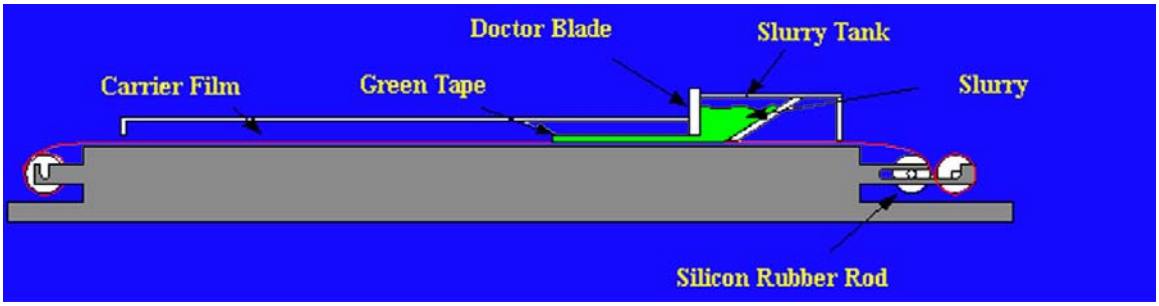

Figure 6. Schematic of a Tape Casting Machine.

CHAPTER 2
PREPARATION OF DENSE BARIUM CERATE FILM ON A PLANAR POROUS SUPPORT FOR HYDROGEN SEPARATION MEMBRANE

Proton conducting ion transport membranes have attracted attention for future fuel processing and energy production systems as well as ancillary technologies such as fuel cells, sensors and electrolyzers. Hydrogen from mixed gas streams during processing of fuels and other petrochemical products has been separated by proton-electron conducting perovskite oxides (93-98). Mixed strontium cerate-zirconate and barium cerate-zirconate based perovskite type oxides exhibit protonic conduction at elevated temperatures in atmospheres containing hydrogen or water vapour (98,99), Figure 7. Multivalent cation doped barium cerate is being studied for its application in hydrogen separation membranes due to its high temperature proton conductivity.

In this study we have made use of the Pechini process and Oxalate coprecipitation methods to produce barium cerate powder. The ratio of metal nitrates to citric acid was varied to test the effect of increase in citric acid on particle size and calcination temperature. Simultaneous differential thermal analysis and thermogravimetry was carried out on the powders which were then calcined and characterized by XRD. Particle analysis was done using BET while the microstructure was studied under SEM.

Experimental

Preparation of Barium Cerate Electrolyte Powders

Powders of barium cerate were made by two processes: Pechini and Oxalate coprecipitation method. In the Pechini process stoichiometric amounts of barium nitrate,

cerium nitrate and citric acid were dissolved in deionised water to which ethylene glycol was later added. The solution was then heated on a hot plate to form a gel which was further heated to burn off the organic constituents. The molar ratio of nitrates to citric acid varied from 1:1 to 1:4 while the ratio of citric acid to ethylene glycol was kept constant. These precursors were then calcined at 1000 ^{o}C for 8 hours to ensure a pure barium cerate phase. Powder preparation using a 1:3:3 ratio was found to be much easier to prepare and hence was used for more tests. In the Oxalate Coprecipitation process barium nitrate and cerium nitrate were dissolved in deionised water, and then heated to boil. Excess hot ammonium oxalate was added to the nitrate solution with vigorous stirring to effect instantaneous coprecipitation. The precipitate formed was kept overnight, filtered and dried in an oven at 110 ^{o}C for 6 hours. The dry powder was calcined for a period of 8 hours at 1100 ^{o}C to get fine barium cerate powder.

Preparation of NiO-GDC substrate

Nickel oxide-gadolinium doped ceria powder was used as a substrate material because of its steam reforming and chemically inactive properties at high temperatures. In Uniaxial press method suitable volume % of nickel oxide and gadolinium doped ceria were ballmilled together in propanol for 24 hours. This solution was dried in an oven and the dry powder pressed in form of round pellets in a die. The pellets were then calcined at 850 ^{o}C.

Preparation of barium cerate and NiO-GDC pellets

The calcined barium cerate powder obtained from oxalate method and calcined NiO-GDC powder from the Uniaxial method was pressed in the form of pellets approximately 13 mm in diameter and 4 mm in thickness. The pellets were sintered at

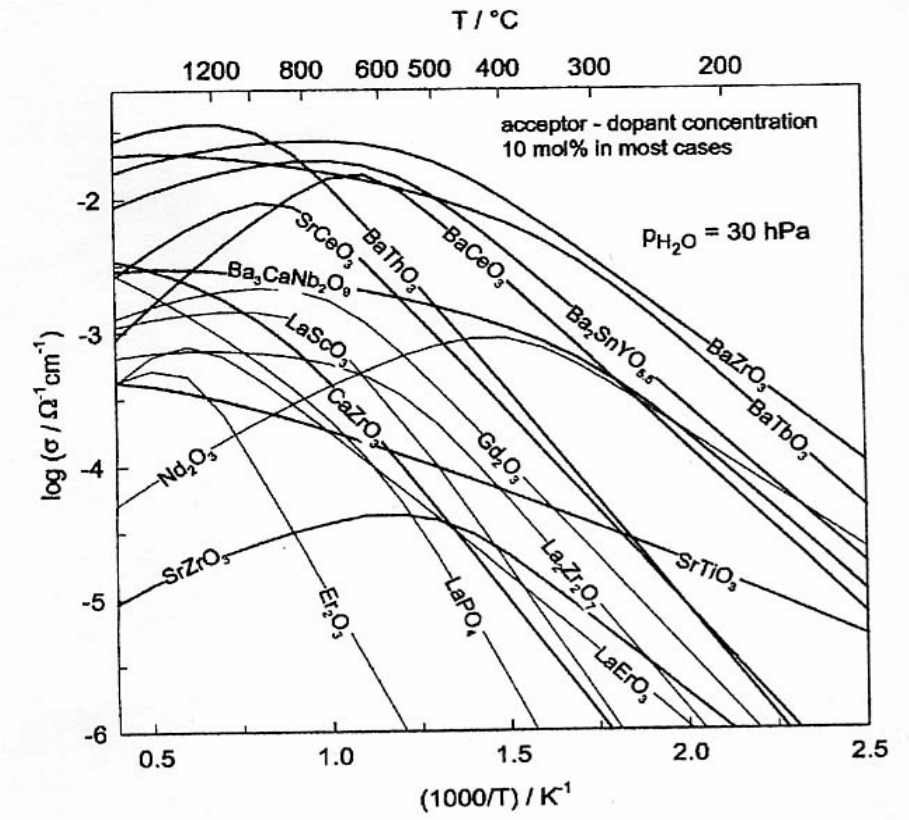

Figure 7. Proton conductivities of various oxides as calculated from data on proton concentrations and mobilities, according to Norby and Larring (type of dopant is not indicated) Conductivities of perovskite type structures are shown by bold lines.

temperatures varying from 1100 ^{o}C to 1600 ^{o}C at an interval of 100 ^{o}C and at the heating rate of 5 ^{o}C/min. The diameter and thickness of each pellet before and after sintering rate of 5 ^{o}C/min. The diameter and thickness of each pellet before and after sintering was measured and shrinkage rate determined for each temperature. A plot of shrinkage rate vs temperature was plotted from this data.

Dipcoating and firing

A colloidal solution was made by dispersing barium cerate powders in propanol and using PVB as the binder. The dispersions stabilized at a pH of about 6.5. The presintered substrates made by Uniaxial method were then dipcoated for a couple of times in the dispersion to get a reasonably thick film and dried in an oven at 70 ^{o}C. The samples using oxalate powder were sintered at 1300 ^{o}C, 1400 ^{o}Cand 1500 ^{o}C at a heating rate of 5 ^{o}C/min for 5 hours while the powder from Pechini was sintered at 1500 ^{o}C at the same firing schedule. Microstructure of the sintered samples was analysed under SEM.

Results and Discussions

Characterization

TGA-DTA Results

TGA-DTA measurements were done on the Pechini powders for analyzing the decomposition of the polymeric precursor and formation of single phase. A heating rate of 10 ^{o}C/min was used. The terms M^{+}, CA, EG stand for metal nitrates, citric acid and ethylene glycol respectively. The stoichiometry for the reaction in Pechini process is 1:1 i.e. one citric acid group chelates one metal ion. Powders were made using different metal nitrates to citric acid ratios. Figure 8 shows the TGA-DTA curves for different

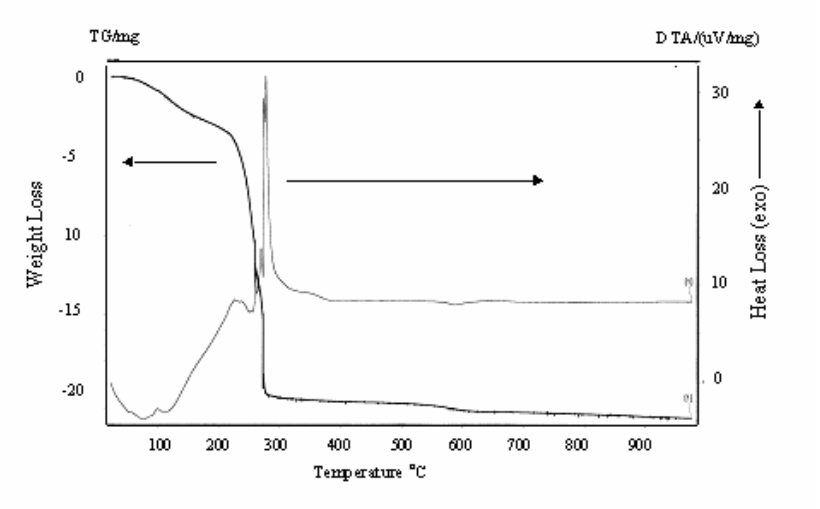

(a) M^+:CA:EG = 1:1:1

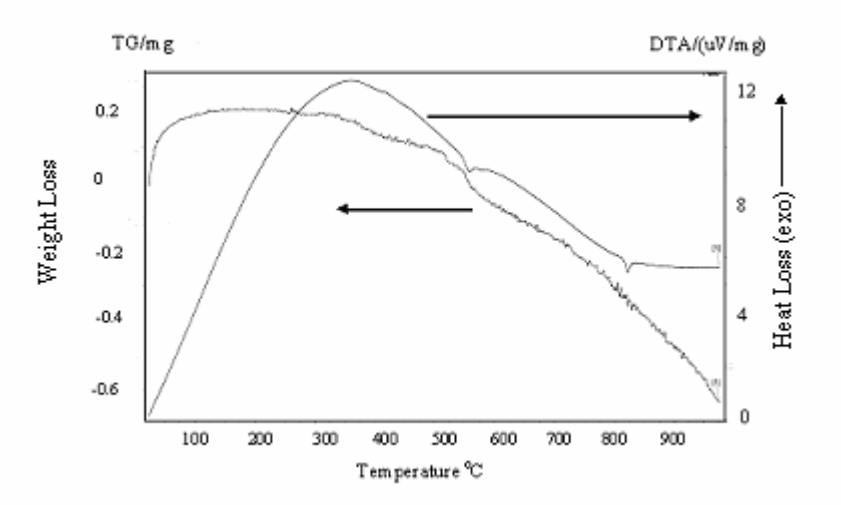

(b) M^+:CA:EG = 1:2:2

Figure 8. TGA-DTA measurements of powders from Pechini process where M^+, CA, EG stand for metal nitrates, citric acid and ethylene glycol respectively. Ratios vary as (a) 1:1:1, (b) 1:2:2, (c) 1:3:3 and (d) 1:4:4.

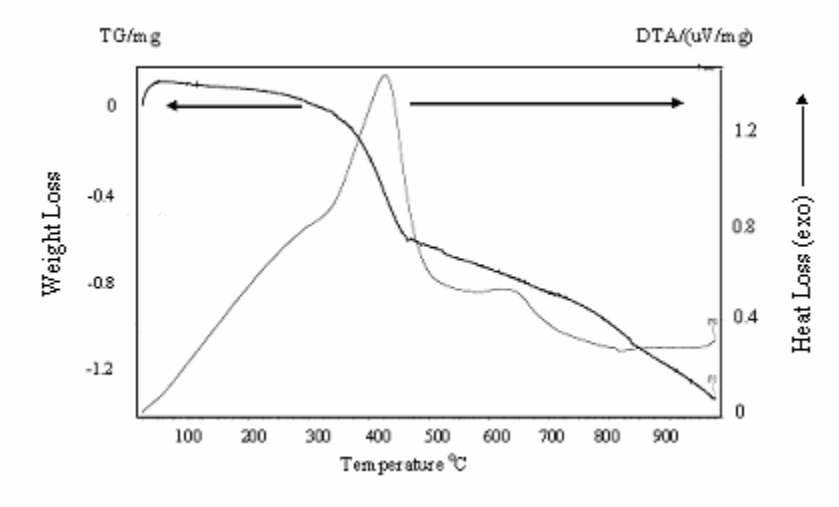

(c) M^+:CA:EG = 1:3:3

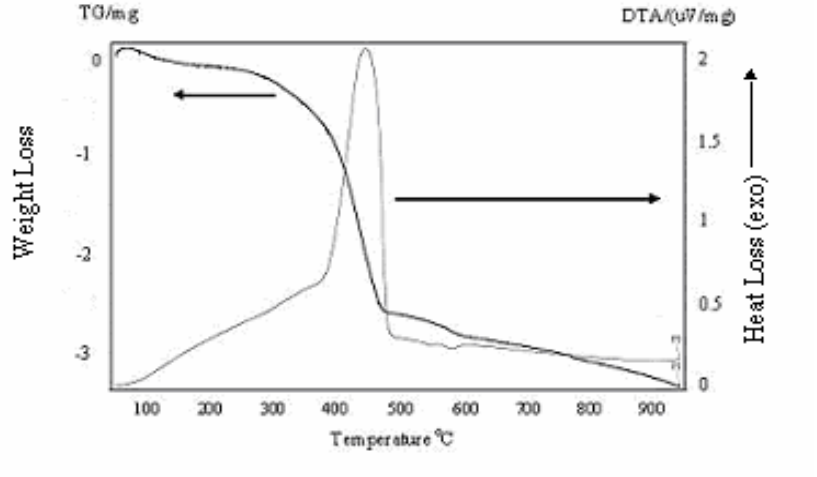

(d) M^+:CA:EG = 1:4:4

ratios of metal nitrates to citric acid. For (a) the stoichiometric composition the precursor was not burnt while the precursors in (b), (c) and (d) were partially burnt i.e. some amount of organic matter in the precursor was burnt off at about 300 ^{o}C for 15 minutes before performing TGA-DTA analysis. In (a) the ratio of nitrates to citric acid is 1:1 while for (b), (c) and (d) it is 1:2, 1:3 and 1:4 respectively. TGA curve shows a complete mass loss by about 300 ^{o}C which could be due to the presence of primarily organics in the precursor. Comparing (b), (c) and (d) it is seen that the heat loss and mass loss was faster as the amount of citric acid increased. Also the organic loss continues even after 600 ^{o}C. This continous mass loss seen after 600 ^{o}C could be due to the evolution of carbonates at high temperatures.

XRD Observations

The XRD spectra obtained by calcining the powder made from 1:3:3 ratio at different temperatures is shown in Figure 9. It is seen that at 700 ^{o}C and 800 ^{o}C there is dominant presence of carbonates and oxides. At 900 ^{o}C there is formation of the primary phase along with some traces of a second phase. At 1000 ^{o}C the second phase completely disappears and formation of barium cerate is complete. Figure 10 shows the XRD spectra for powders made using different amounts of citric acid, also calcined at 1000 ^{o}C to determine if a single phase was obtained in all cases. The 1:1 ratio shows presence of second phase even at 1000 ^{o}C while for powders from the 1:2 and 1:4 ratio barium cerate is formed at 1000 ^{o}C. Powder from oxalate method was also calcined at different temperatures and it was observed that single phase is obtained at 1100 ^{o}C as seen in Figure 11.

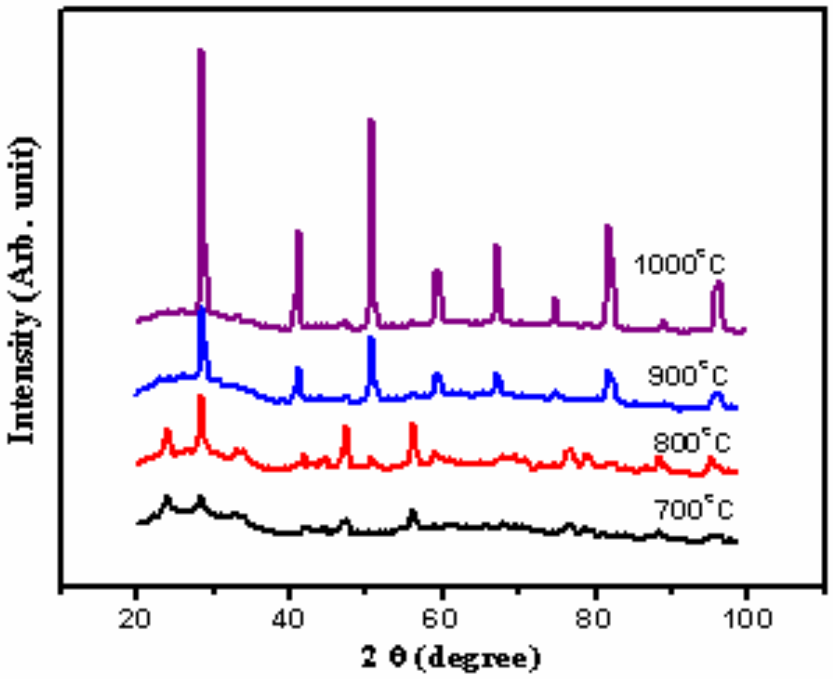

Figure 9. XRD spectra for powders made by Pechini process using M+:CA=1:3 and calcined at different temperatures

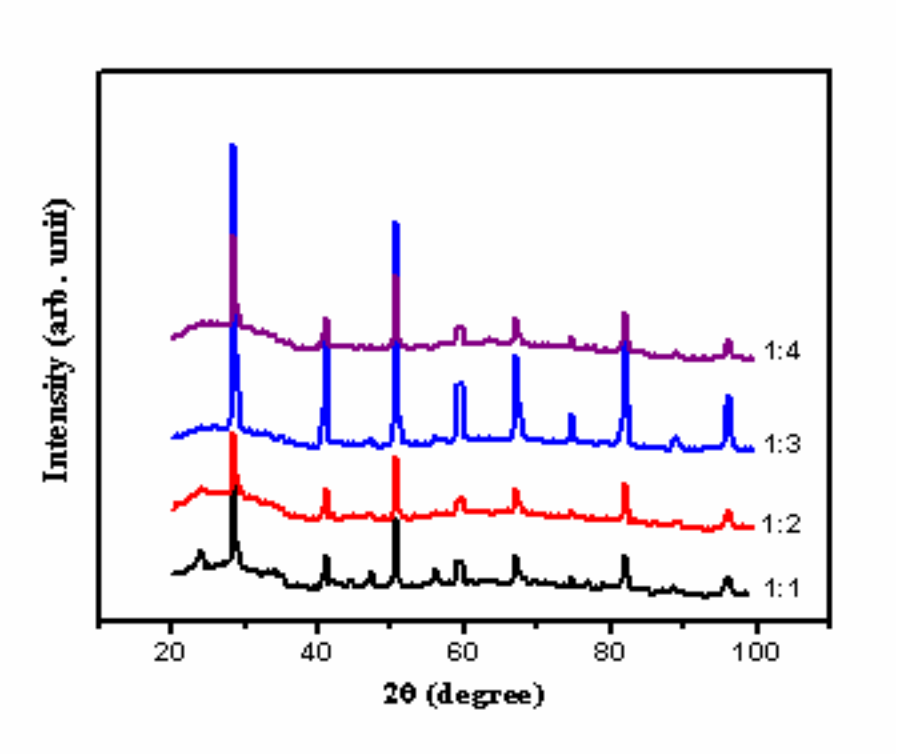

Figure 10. XRD spectra according to content of citric acid in powders calcined at 1000 ^{o}C.

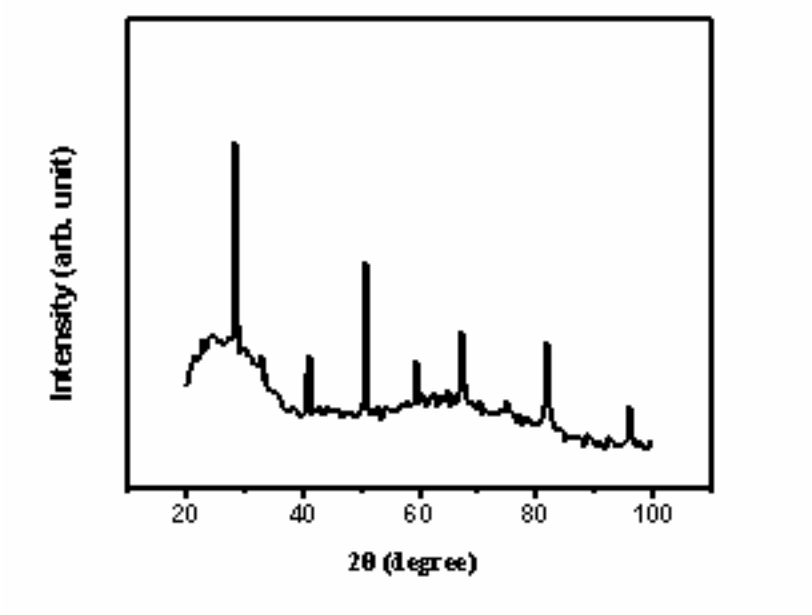

Figure 11. XRD spectra for powder calcined at 1100 ^{o}C by Oxalate method

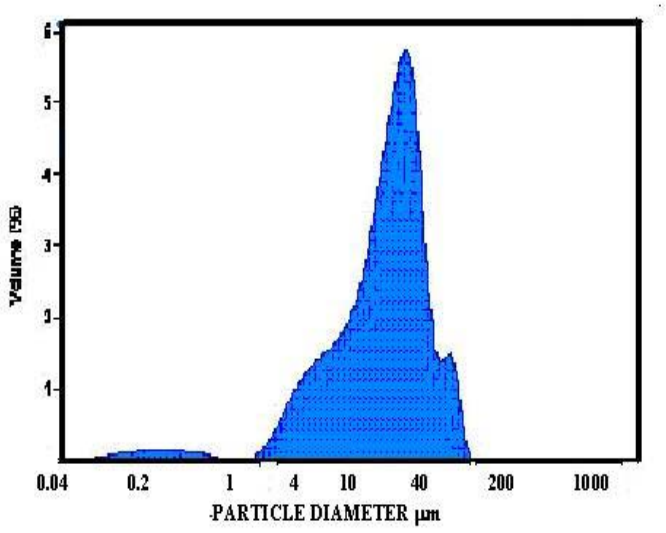

Figure 12. Particle size distribution for powder calcined at 1100 ^{o}C from oxalate method.

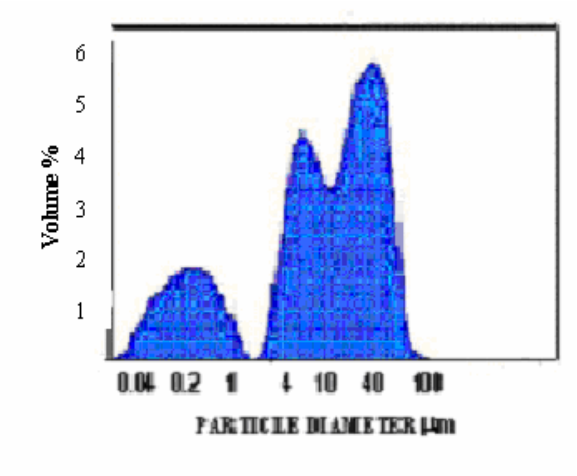

M^+:CA=1:1

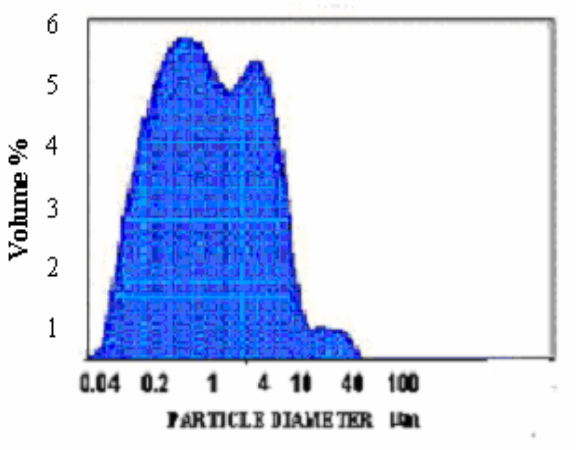

M^+:CA=1:2

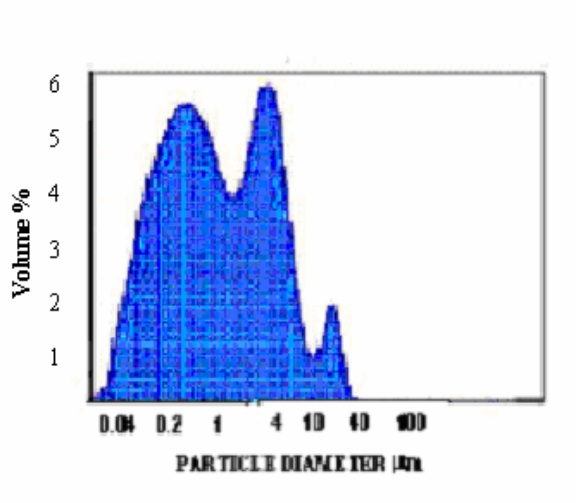

M^+:CA=1:3

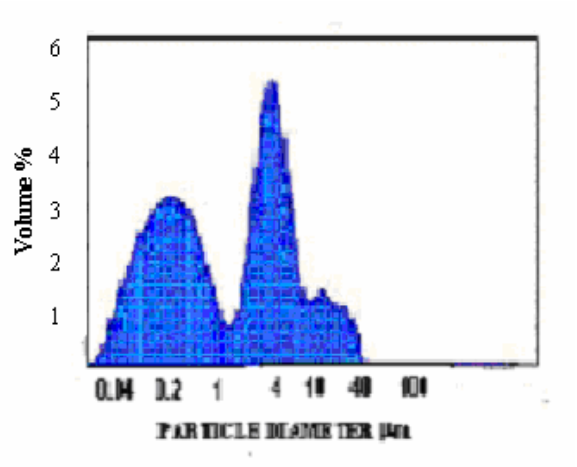

M^+:CA=1:4

Figure 13. Particle size distribution for Pechini powder calcined at 1000 ^oC for various M^+:CA ratios

Particle Size distribution

A smaller grain size and large grain boundary is desirable for good sintering kinetics. Figure 12 shows the distribution for the Oxalate powder. Figure 13 shows the particle size distribution of powders after calcining from the Pechini process. Judging from the curves obtained for different amounts of citric acid it is seen that for1:1 ratio of nitrates to citric acid the particle size distribution is the largest while it decreases for higher amounts of citric acid. A bimodal size distribution is observed for 1:1 and 1:4 ratios of nitrates to citric acid. Comparing the distribution of the particle size from both methods it is observed that Oxalate method yields larger particle size.

Determination of optimum sintering temperature and microstructure of film

Mismatch in shrinkage rate between the film and the substrate is one of the important reasons as to why films are obtained with cracks, warpage or other deformities. Shrinkage rate varies not only because each material has a different thermal history but also due to the presence of organic matter used while synthesizing the material. So it is necessary to estimate the shrinkage rate of the film and substrate so as to arrive at an optimum sintering temperature where the effects of shrinkage would be minimal. Figure 14 shows the plot of shrinkage rate % vs temperature for barium cerate and NiO-GDC powder. All the curves run parallel to each other. The barium cerate curve appears to deviate at around 1500 ^{o}C and it could be due to experimental error or some other reasons. So following the curve trend a temperature of 1500 ^{o}C was assumed for sintering of the dipcoated film. The idea was that since the curves deviate at about 1500 ^{o}C there would be a shrinkage mismatch above this temperature which would lead to defects in the film.

Figure 15 and 16 show the surface view of the films from oxalate method sintered at 1300 ^{o}C and 1400 ^{o}C. Figure 17 and 18 show the surface and cross sectional view of film at 1500 ^{o}C made from Oxalate method while Figure 19 and 20 from the Pechini process sintered at 1500 ^{o}C. Below 1500 ^{o}C a porous microstructure is observed in the film. But as the sintering temperature is increased the grains grow and increased density of film is observed. The grain size in case of Oxalate powder is much larger as compared to the Pechini powder. This could be due to the larger initial particle size of the powder obtained from the Oxalate method. The film is more dense at 1500 ^{o}C but still shows presence of scattered pores in both cases. The thickness of the film is about 7-10 μm for both the powders.

Conclusions

Barium cerate was prepared by Pechini and Oxalate coprecipitation method. A single phase was obtained at 1000 ^{o}C for powder from Pechini process and at 1100 ^{o}C for Oxalate process. Oxalate method gave a larger particle size distribution which was also reflected in the microstructure of the film in form of larger grain size compared to Pechini method. Increase in sintering temperature lead to increase in grain growth and increased density of film and the pores were limited to grain boundaries. A dense film was obtained at 1500 ^{o}C.

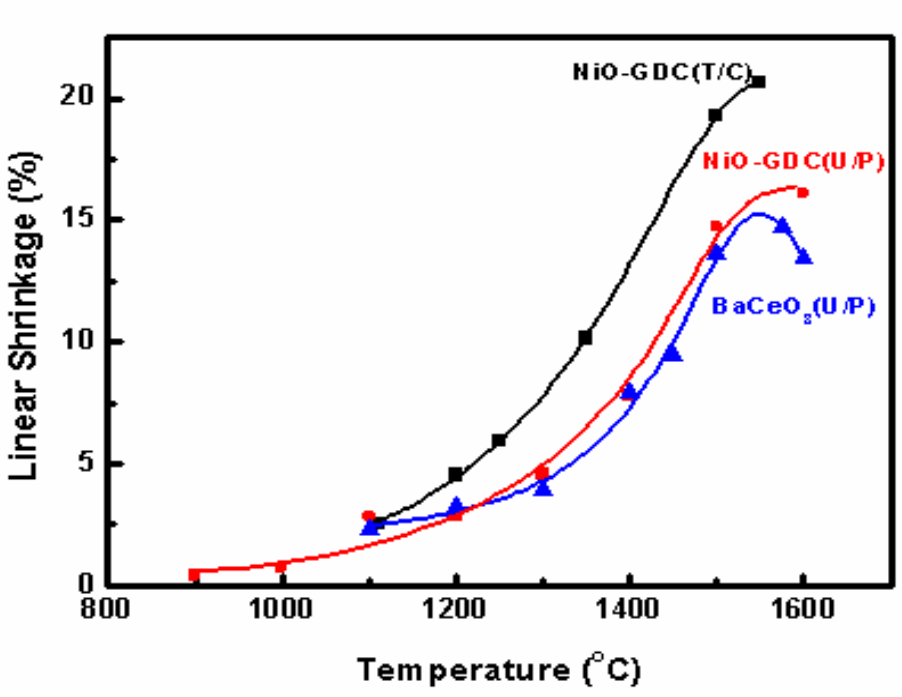

Figure 14. Shrinkage rate % vs Temperature between $BaCeO_3$ and NiO-GDC powder prepared by Uniaxial (U/P) and Tape casting (T/C) method.

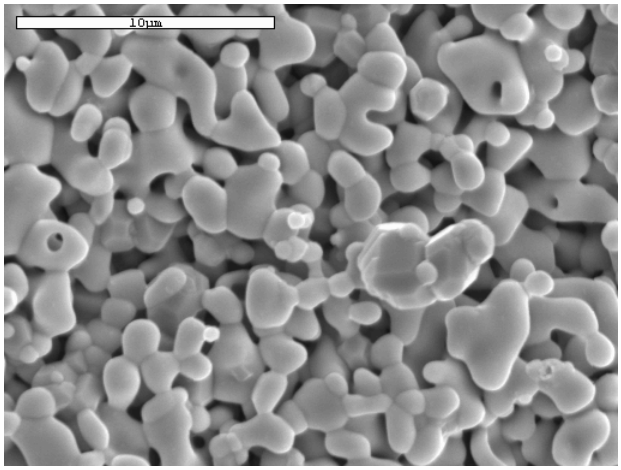

Figure 15. Surface view of film from oxalate powder sintered at 1300 ^{o}C

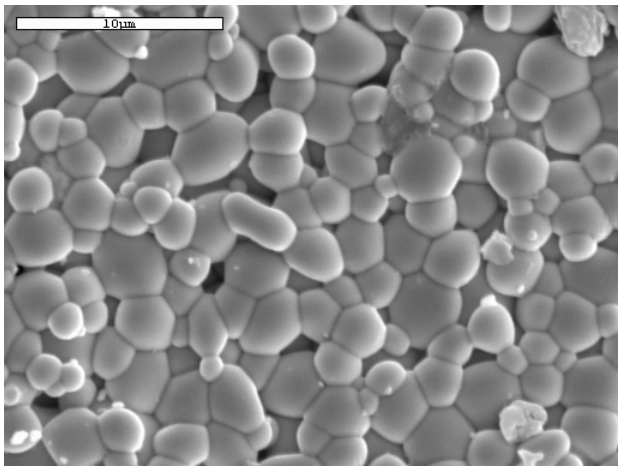

Figure 16. Surface view of film from oxalate powder sintered at 1400 ^{o}C

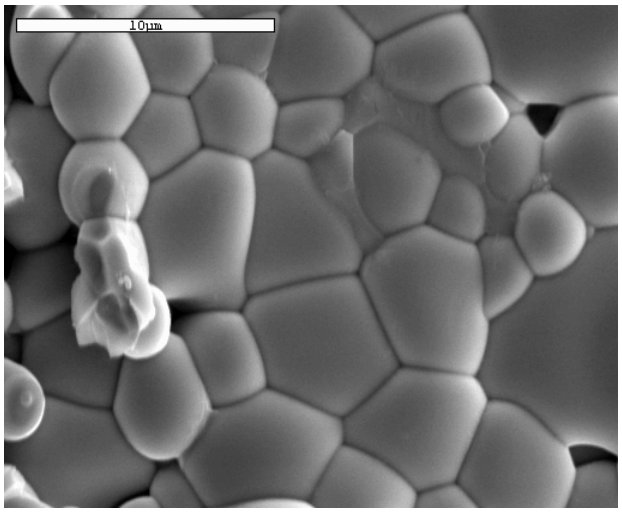

Figure 17. Surface view of film from oxalate powder sintered at 1500 ^{o}C

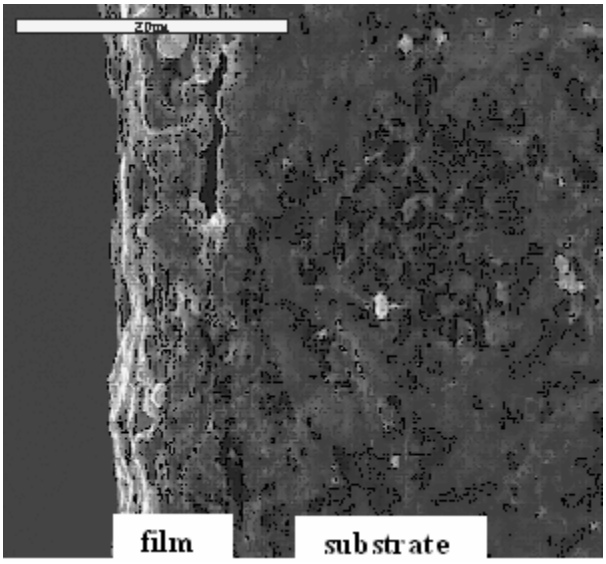

Figure 18. Cross-section view of film from oxalate powder sintered at 1500 ^{o}C

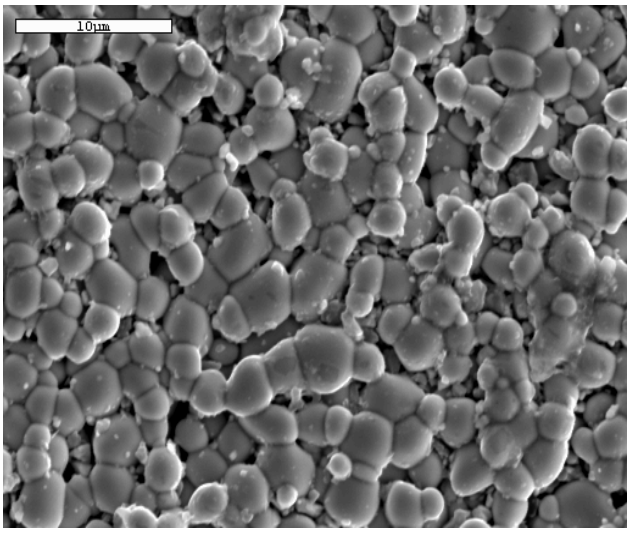

Figure 19. Surface view of film from Pechini powder sintered at 1500 ^{o}C

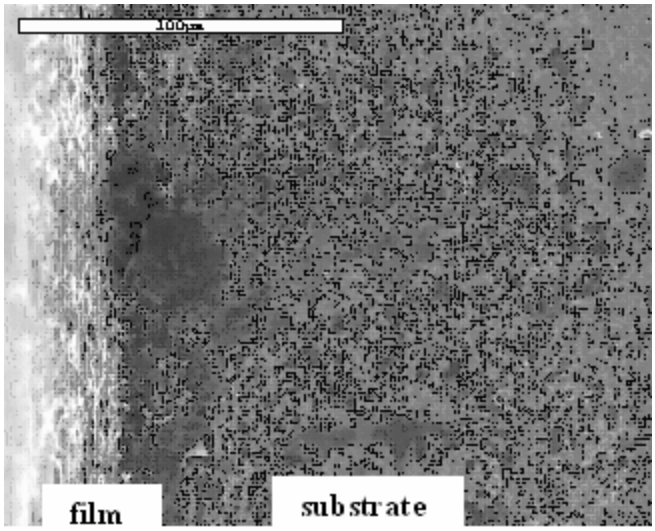

Figure 20. Cross-section view of film from Pechini powder sintered at 1500 ^{o}C

CHAPTER 3
PREPARATION OF DENSE EUROPIUM DOPED BARIUM-CERATE FILM ON A PLANAR POROUS SUPPORT FOR HYDROGEN SEPARATION MEMBRANE

In the previous work barium-cerate powder was made using Oxalate and Pechini process. A film was deposited on a nickel oxide-gadolinium doped ceria substrate using a dipcoating method. Analysis of shrinkage rates of the film and substrate material showed that their shrinkage rates matched at around 1500 ^{o}C and so the films were sintered at 1500 ^{o}C. The next stage of experiments involve using europium as a dopant. Doped substances can exhibit different properties than the undoped material and unique applications may be possible only in the doped system. Dopants may be added to impart ionic or electronic conductivity, to make the membrane permeable to a specific gas etc. so that it can be used for various applications. A multivalent dopant can impart electronic conductivity. For ionic conductivity acceptor or donor dopant (e.g., Sm^{3+} is an acceptor dopant for CeO_2) can be used. For permeation both, electronic & ionic conductivity is required. Barium cerate already has some ionic conductivity and adding europium cation does 2 things (1) since it has lower valence states than Ce^{4+} it acts as an acceptor and creates more vacancies, and (2) since it is multivalent, it creates electronic species by going from Eu^{3+} to Eu^{2+} thereby increasing electronic conductivity. So permeation can be obtained by using europium as dopnat in the barium cerate system.

Following stages were involved :

- -Preparation of Eu doped barium cerate powder.
- -Determining the actual % of Eu in the calcined powder using EPMA.

- -Slurry preparation of the same.
- -Coating of slurry on tape casted substrate by spin coating.
- -Sintering and studying the microstructure of the film.
- -Testing for hydrogen permeation.

Substrates made by tape casting were used instead of those made by Uniaxial press. Figure 21 shows the flow chart of the experimental method to prepare the same.

Experimental

Preparation of Eu Doped Barium Cerate Powder.

Stoichiometric amounts of barium nitrate, cerium nitrate and europium nitrate in the molar ratio Ba:Ce:Eu = 1:0.85:0.15 were dissolved in distilled water. Ammonium oxalate was dissolved separately, heated to about 100 ^{o}C and added to the nitrate solution. The precipitate formed was allowed to stand overnight and later filtered and dried. The powder was then calcined at 1200^{o}C. Formation of single phase was determined using XRD. Pechini process was also tried to synthesize the powder but the solution did not polymerize under any condition and so doped powder could not be made by this route.

The actual % of europium present in the synthesized powder was determined using EPMA(Electron Probe Micro-Analysis). For this the calcined powder was pressed in the form of a pellet and sintered at 1500 ^{o}C. The results showed that Eu was approximately 12 % instead of 15 % and the amount of barium was also less by 3-4 % than originally started with. This reduction in barium content can be attributed to the fact that the high vapour pressure of barium oxide caused it to evaporate at 1500 ^{o}C. The reduction in the amounts of the europium and barium can also be understood through Porbaix diagrams. From figure 5 it is clear that all the metal cations do not precipitate at the same time and hence the results with amounts lesser than actually started with.

Slurry preparation and Spin coating

The composition of the slurry is very important to achieve a desired viscosity for spin coating. After some trial and errors a final slurry was made using the following composition, Table 2, and ballmilled for 24 hours.

Table 2. Composition of slurry for spin coating

MATERIAL	AMOUNT IN GRAMS
Eu doped barium cerate powder	5
Di butyl pthalate(DBP)	0.5
Polyvinyl butyral(PVB)	0.2
Ethanol+Toluene soln	1.5 each

PVB acts as a binder in this case while DBP functions as a plasticiser. The amount of plasticiser is very important since it directly affects the flow properties of the slurry. Ethanol and toluene were added in equal amounts to dissolve the PVB as well as impart sufficient viscosity to the slurry.

The tape cast substrates were then coated with the slurry using the spin coating method. The substrates were presintered at two temperatures, 1250 ^{o}C and 1550 ^{o}C. The film was sintered at1400 ^{o}C , 1450 ^{o}C and 1500 ^{o}C.

A slurry was also prepared by adding PVB only as the binder to the doped barium cerate –ethanol solution. A film was deposited by spin casting on tape cast and uniaxially pressed substrates.

Doped barium cerate powder was pressed in the form of pellets and sintered at 1500 ^{o}C and 1600 ^{o}C for different hold times to study the densification behaviour.

Testing for hydrogen permeation

A sample made by depositing film on uniaxially pressed substrate was about 1 inch in diameter so that it could sit properly on the furnace tube and could be sealed properly to conduct the permeation test. Before the actual permeation the sample was heated to 800 ^{o}C

and hydrogen was allowed to flow at a ramp rate of 10ccm for 6 hours. The sample was allowed to cool in hydrogen atmosphere. Helium was used as the sweep gas for the permeation experiment. The sample was sealed on a glass tube at a temperature of 875 ^{o}C. After cooling the sample was tested for gas leakage at 850 ^{o}C using a mixture of helium and argon gas.

Results and Discussions

Figures 22, 23 and 24 show the surface view of films sintered at 1400 ^{o}C, 1450 ^{o}C and 1500 ^{o}C and the substrate presintered at 1250 ^{o}C. Comparing the three figures show that the grain size varies from 2-5 μm at lower sintering temperatures but becomes more uniform as sintering temperature is increased. The grain size at 1500 ^{o}C is about 2μm. Few pores are seen in Figure 24 as compared to Figure 22 and 23 which shows that density of the film also increases with increase in the sintering temperature. Figure 25 shows the cross sectional view of film sintered at 1500 ^{o}C. The thickness of the film is about 10μm. Warpage was observed in all the three films due to thermal mismatch between the film and substrate material. Figure 26 shows the film sintered at 1450 ^{o}C but with the substrate presintered at 1550 ^{o}C. The film is porous but no warpage was observed in this case.

Figure 27 shows the film microstructure on a uniaxially pressed substrate which was presintered at 1250 ^{o}C . The film is highly porous even at sintering temperature of 1500 ^{o}C. Figure 28 shows the porous cross section of the same. There was warpage observed in this case also which was concave in nature Vs the convex warpage in case of tape cast substrates. The film from tape cast substrate looks dense with intermittent cracks as seen in Figure 29 at a low resolution. At higher resolution it is seen that the film is composed of dense patches which are separated by cracks. At places where pores are seen there is also an underlying

layer of film so the pores are not interconnected, Figure 30. The cross-section shows the film to be around 10 μm thick, Figure 31.

Barium cerate densifies by the solid state sintering mechanism and so it is very difficult to obtain a dense film on a substrate. Figures 32 and 33 show barium cerate sintered at 1500 ^{o}C and held for 5 and 8 hours while Figure 34 and 35 at 1600 ^{o}C for 5 and 8 hours respectively. At 1500 ^{o}C the material densifies by solid state sintering but as the temeparture and holding time are raised some melting of the material is observed. Liquid phase sintering is observed at 1600 ^{o}C but it does not seem to occur uniformly as is evident from Figure 34. This could be responsible for the presence of pores even at these temperatures. More higher temperatures and holding time may be required to complete the sintering process so as to obtain a completely dense film. Another way could be to add a sintering aid which melts at lower temperature so that it would fill up the pores created during the sintering process.

In case of permeation argon was present in the sweep gas indicating that the film was porous which allowed the gas to permeate through. So film deposited on uniaxially pressed substrate was porous. Samples could not be made using tape cast substrates for permeation because the samples broke on sintering. Therefore hydrogen permeation results could not be obtained.

Conclusions

Europium doped barium-cerate powder was prepared by Oxalate Coprecipitation method since the Pechini process was not successful in synthesizing doped powder. EPMA technique was used to determine the amount of europium in the sintered powder which was about 12 % as compared to the 15 % added during preparation of the doped powder. Films obtained from europium doped powder were more dense than the undoped ones. Films made from slurry looked dense but the results could not be reproduced since a stable slurry was not

formed later on. It could be due to some contamination or change in temperatures. A simple slurry consisting of binder, powder and ethanol was made and coated on tape cast substrate which gave a relatively dense film compared to the film obtained on uniaxially pressed substrate. This difference could be due to the different shrinkage rates in both cases. Film on tape casted substrate was quite dense but with presence of cracks and pores. This means that the composition of the substrate needs to be varied so as to accommodate the shrinkage rate of the film material so that it does not crack. GDC is inactive at temperatures of 1500 ^{o}C so the nickel is basically affecting the shrinkage. So nickel % can be reduced and see if it makes any difference. Sintering temperatures of more than 1500 ^{o}C with high holding times can be used so as to cause densification by liquid phase sintering as well. This might also ensure the complete removal of pores and a completely dense film. Stress caused due to too fast or too slow heating and cooling rate can also give rise to cracks. Presence of argon in sweep gas during the permeation tests indicated that the film was porous. So hydrogen permeation results could not be obtained.

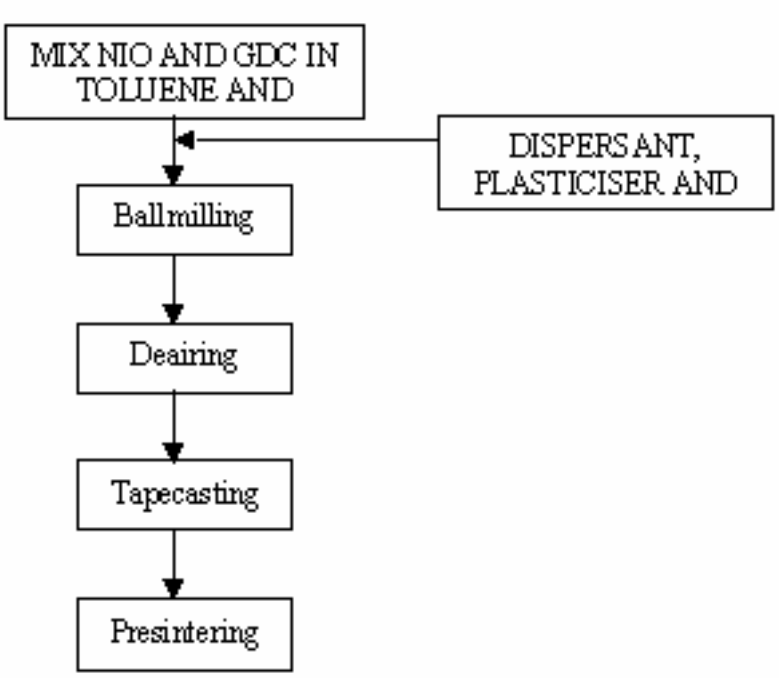

Figure 21. Flow chart for preparation of Tape Cast substrates.

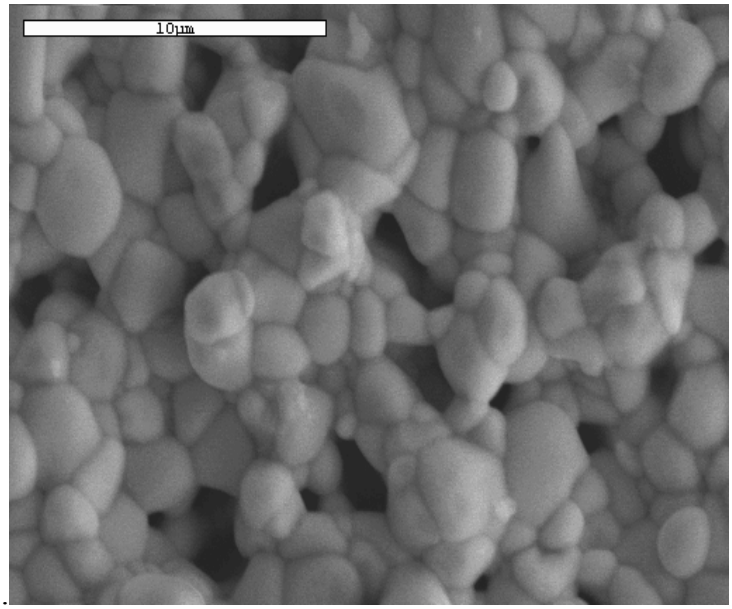

Figure 22. Surface view of spin coated film sintered at 1400 ^{o}C on tape cast substrate

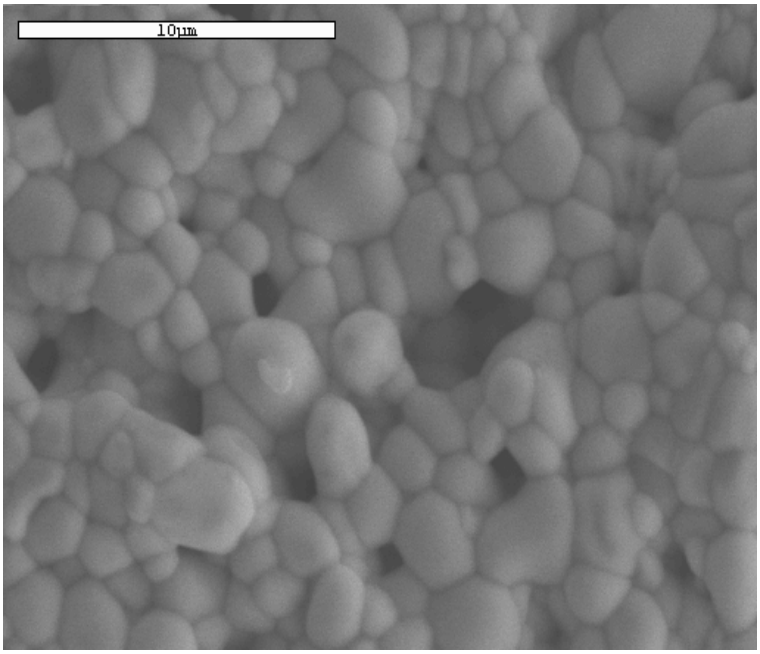

Figure 23. Surface view of spin coated film sintered at 1450 ^{o}C on tape cast substrate

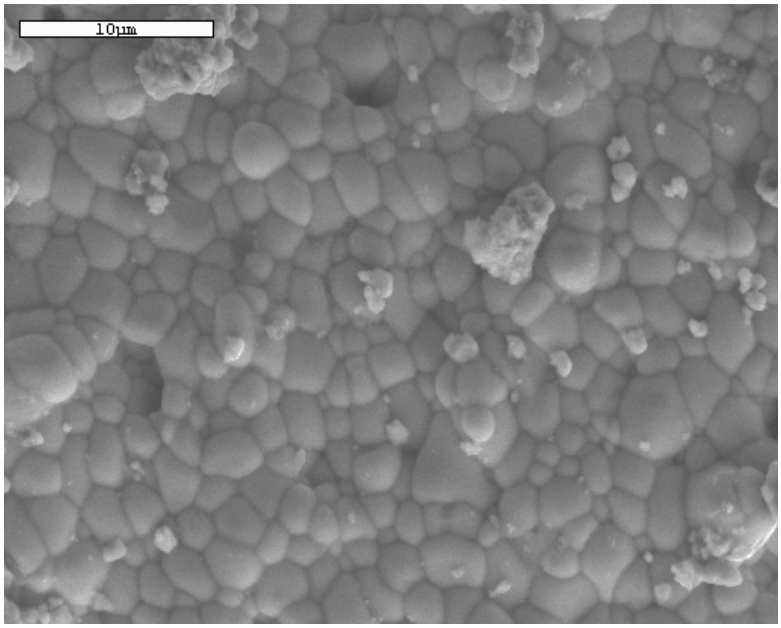

Figure 24. Surface view of spin coated film sintered at 1500 ^{o}C on tape cast substrate

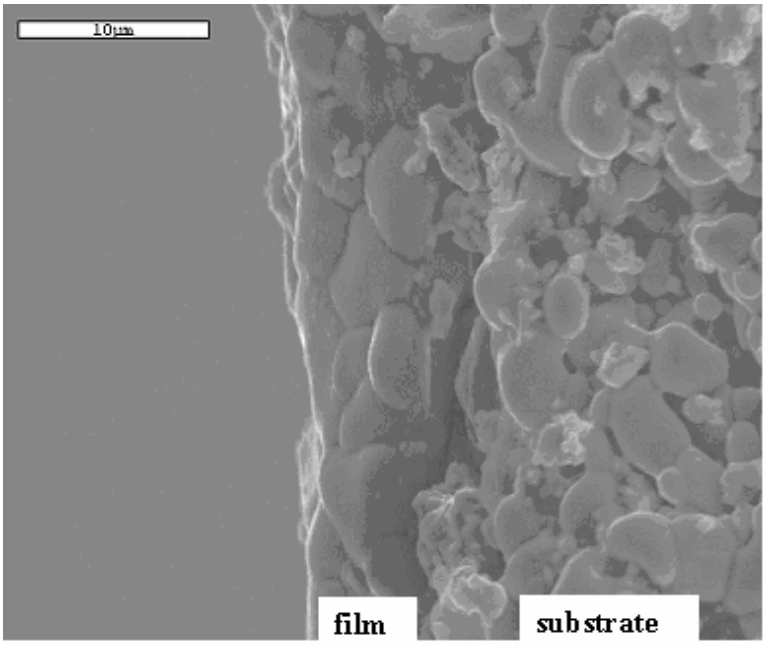

Figure 25. Cross-section view of spin coated film sintered at 1500 ^{o}C on tape cast substrate

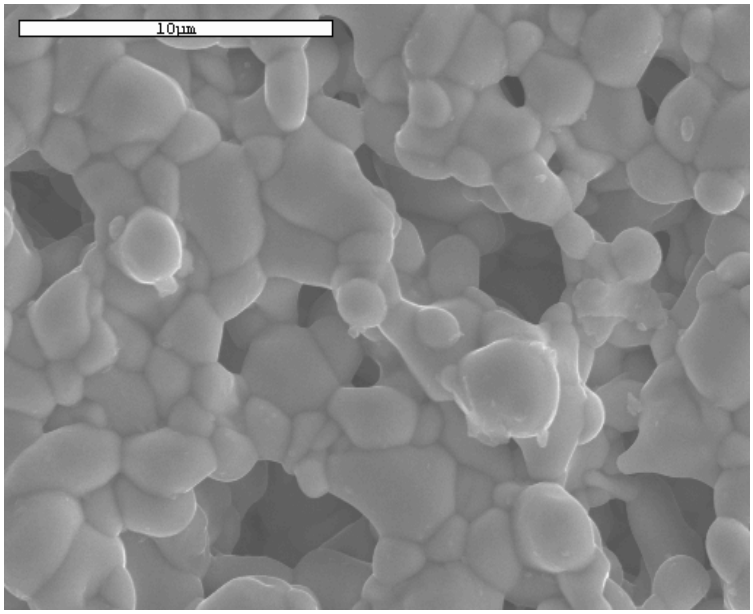

Figure 26. Surface view of spin coated film sintered at 1400 ^{o}C on tape cast substrate (substrate sintered at 1550 ^{o}C)

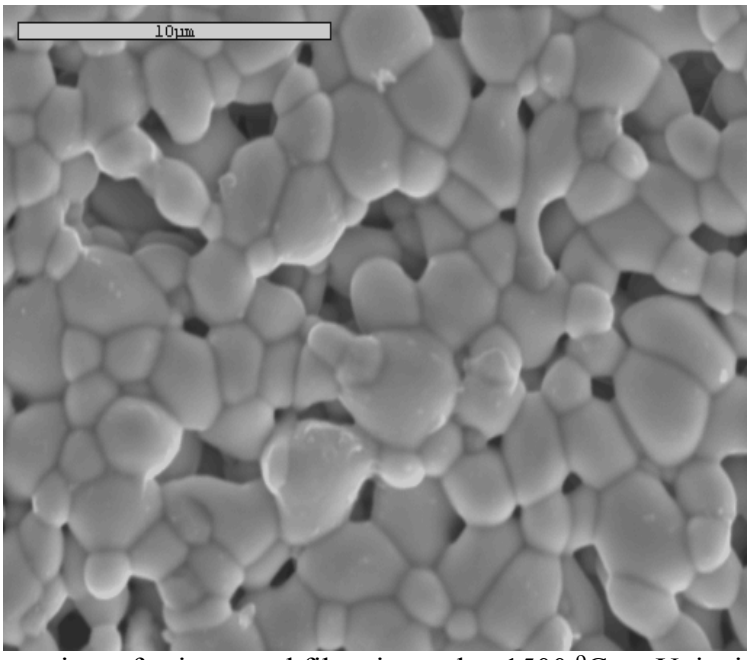

Figure 27. Surface view of spin coated film sintered at 1500 ^{o}C on Uniaxially pressed substrate

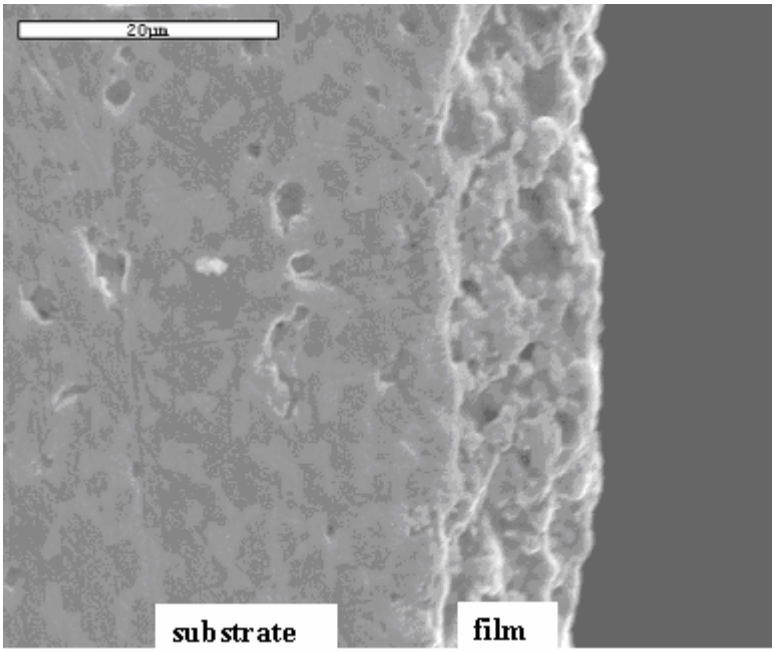

Figure 28. Cross-section view of spin coated film sintered at 1500 ^{o}C on Uniaxially pressed substrate

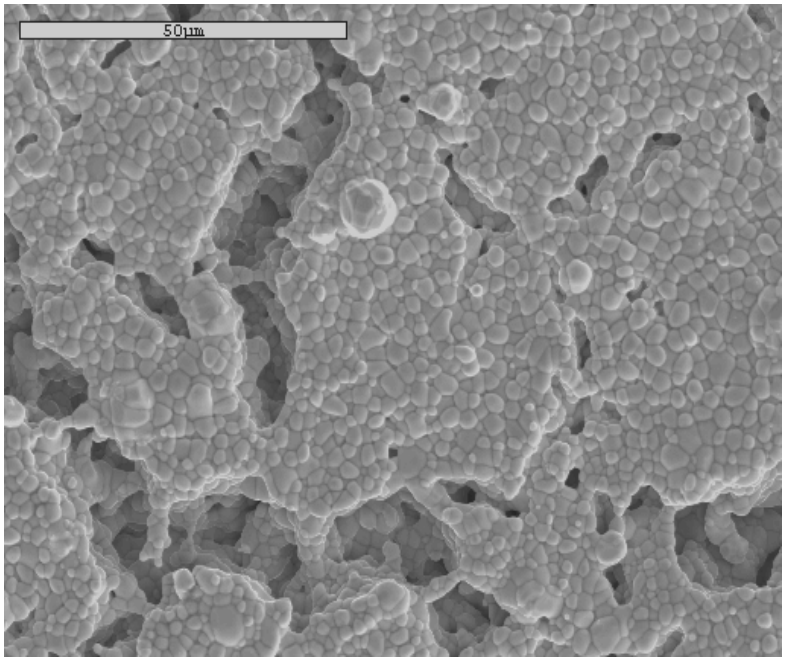

Figure 29. Surface view of spin coated film sintered at 1500 ^{o}C on tape cast substrate (1000X)

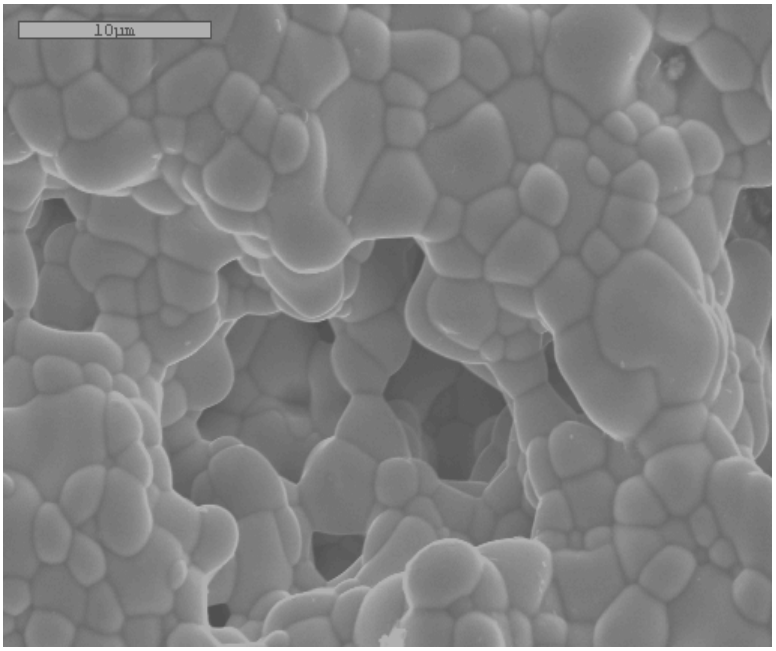

Figure 30. Surface view of spin coated film sintered at 1500 ^{o}C on tape cast substrate (5000X)

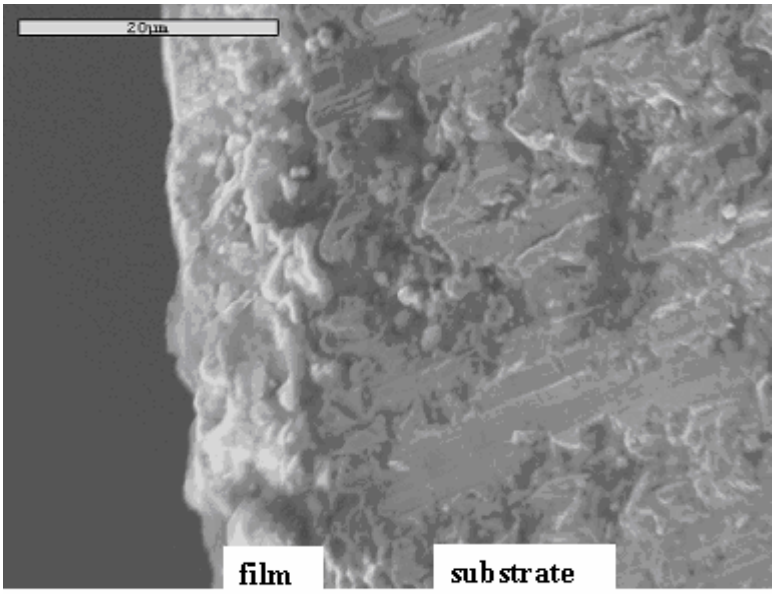

Figure 31. Cross-section view of spin coated film sintered at 1500 ^{o}C on tape cast substrate

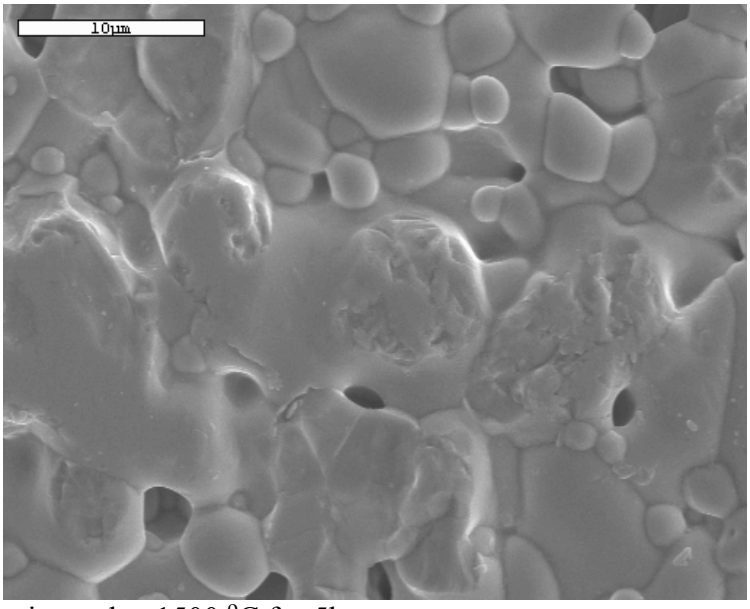

Figure 32.. Film sintered at 1500 ^{o}C.for 5hours

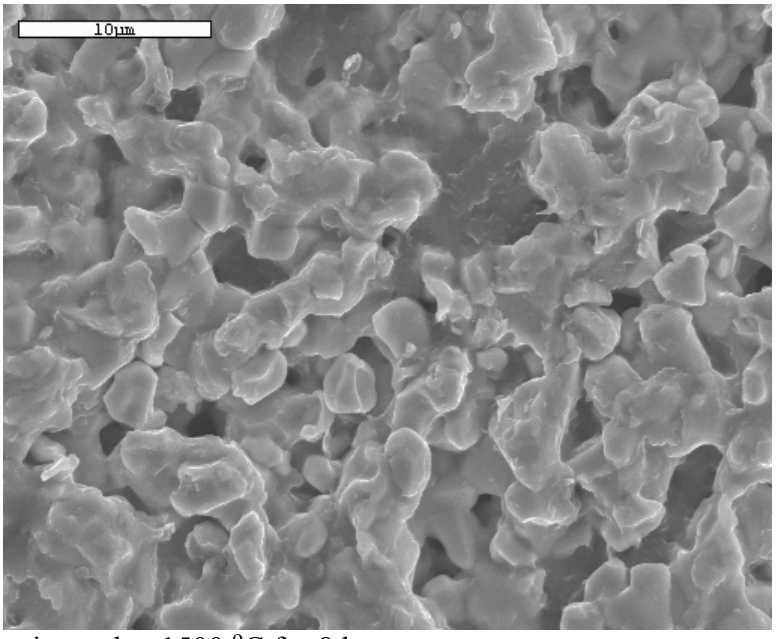

Figure 33. Film sintered at 1500 ^{o}C for 8 hours.

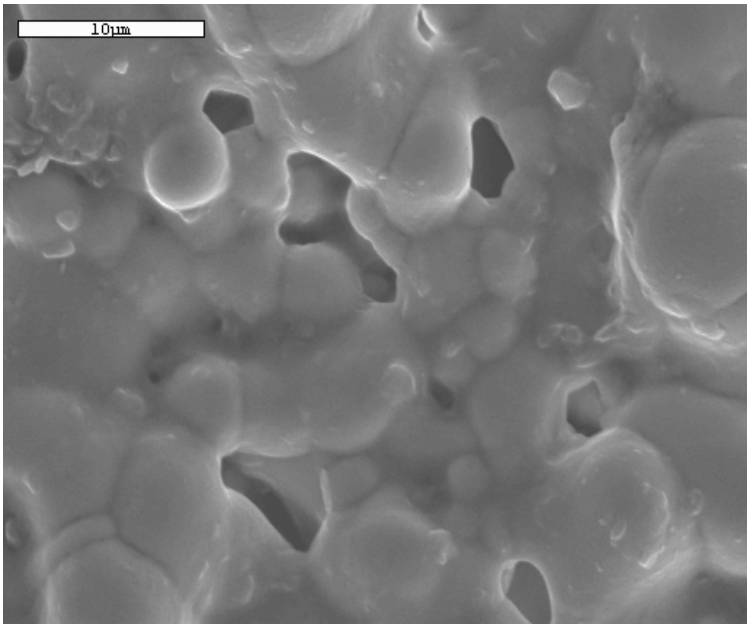

Figure 34. Film sintered at 1600 ^{o}C for 5 hours

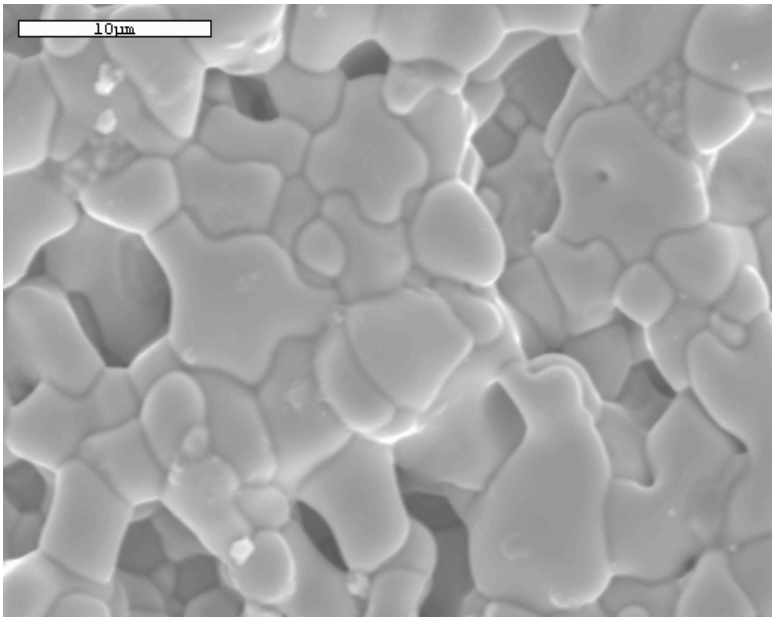

Figure 35. Film sintered at 1600 ^{o}C for 8 hours.

CHAPTER 4
CONCLUSIONS

Undoped and europium doped barium cerate powder was prepared using the Oxalate Coprecipitation and Pechini methods. The powder was characterized using XRD, BET Coulter, TGA-DTA etc. Films were deposited on uniaxially pressed and tape cast substrates by dip coating and spin coating methods.

The Oxalate process gave larger particle size compared to Pechini process. Pechini process involves polymerization of reactants while oxalate precipitation is a chemical reaction brought about by mixing of two solutions where a crystallization process is initiated for precipitation to occur. When precipitation begins microcrystals are formed which serve as seed nuclei for further crystallisation on surface of microcrystals. So there is agglomeration of particles during precipitation which results in larger particle size which is also confirmed by the SEM pictures. Different amount of citric acid used in synthesizing the powder gave varied particle size distribution. Higher calcination temperature was required to form a single phase powder from oxalate method since some unreacted oxalates might be present. Sintering temperatures of 1500 ^{o}C gave a relatively dense film on a tape casted substrate compared to one on uniaxial substrate. This could be due to more uneven shrinkage between the film and substrate material in the later case. Temperatures below 1500 ^{o}C gave porous films which suggested that a higher temperature is necessary for densification of the film. Film densification occurred mainly by solid state sintering which explains the presence of pores in the film. If the

temperature is increased so as to induce liquid phase sintering it might be possible to obtain completely dense films.

A number of factors such as binder content, substrate composition, substrate presintering temperatures, final sintering temperature, holding time, incomplete deairation, composition and viscosity of the solution etc. could affect the final microstructure of the film. Insufficient amount of binder content does not allow the film to adhere properly to the substrate and may peel off after sintering while a high binder content will introduce large amount of organic material which after burning out may result in a porous film. It is necessary to use a substrate material that does not react with that of the film at high temperatures as well as exhibits a shrinkage behaviour similar to the film material. Different shrinkage behaviour results in warpage and cracked films. If substrate is presintered at low temperature it may not be strong enough and may break during deposition of film or final sintering. Final sintering temperature and holding time is important to ensure complete densification by completion of sintering processes and avoid defects in the film.When preparing the slurry for film deposition it is ball milled to get a homogeneous mixture and to remove any air bubbles introduced during the mixing process. Incomplete deairation is when these bubbles are not completely removed and are deposited on the substrate. These air pockets can hinder the complete densification of film. A low viscosity may cause running away of the solution from the substrate while too high viscosity might prevent uniform deposition. So viscosity has to be maintained properly for proper deposition of film. Different binders, plasticizers, solvents etc. are used to prepare slurry. These can drastically affect the flow properties of the slurry if not

used in the proper amounts. So a lot of factors need to be controlled to get a dense, defect free film.

Considering the above factors and the results obtained in the lab it is possible to synthesize undoped barium cerate by Pechini and Oxalate process at calcining temperatures of 1000 ^{o}C and 1100 ^{o}C respectively. As for synthesizing europium doped barium cerate only the oxalate method was successful. A single phase is formed at about 1300 ^{o}C. A binder content of about 0.2 grams for a powder of 5 grams is sufficient to eliminate peel off of the film from the substrate. Nickel oxide-gadolinium doped ceria acts as a good substrate material for depositing barium cerate film. A presintering temperature of 1250 ^{o}C for the substrate is sufficient to impart enough green strength so that it does not crack when film is deposited on it. While preparing the slurry for spin coating a deairation time of 12 hours is sufficient to remove air bubbles from the solution. A final sintering temperature of 1500 ^{o}C can give a dense film with some porosity so higher temperatures should be studied to see if porosity can be completely eliminated.

LIST OF REFERENCES

1. Hydrogen Works, Introduction to Hydrogen, www. Hydrogen.com/intro.html, 1/20/2004

2. Basic Energy Sciences Advisory Committee, Development of an Atomistic Understanding of High Temperature Hydrogen Conductors, Washington DC, May 2002.

3. Alternative Fuel vehicle Group, Report on Hydrogen Economy, December 2003 www.altfuels.com/news.php, 1/20/2004

4. H. Iwahara, K. Uchida, K.Ogaki, J. Electrochem . Soc., 135 (1988) 529.

5. K.D. Kreuer, Solid State Ionics (1997), 97, 1.

6. N. Bonanos, B. Ellis, K. S. Knight, M. N. Mahmood, Solid State Ionics (1989), 35, 179.

7. N. Bonanos, Solid State Ionics (1992), 53-56, 967.

8. N. Bonanos, J. Phys. Chem. Solids, 54 (1993) 867.

9. H. Iwahara, H. Uchida, K. Morimoto, J. Electrochem. Soc., 137 (1990) 462.

10. D. Shima, S. Haile, Solid State Ionics, 97 (1997) 443.

11. T. Yajima, H. Iwahara, Solid State Ionics (1992), 50, 281.

12. K. Liang, A. Nowick, Solid State Ionics, 61 (1993) 77

13. T. Norby, Solid State Ionics (1990), 40/41, 857.

14. N. Bonanos, K. Knight, B. Ellis, Solid State Ionics, 79 (1995) 161.

15. S. E.Roark, R. Mackay, A. F.Sammells, DOE/NETL Contract No. DE-FC26-00NT40762, Eltron Research, Inc., Boulder, 6/11/2002

16. S. J. Visco, C. Jacobson, L. Jonghe, US-DOE Contract DE-AC03-76SF00098.Lawrence Berkeley National Laboratory, San Francisco, December 2002.

17. F. Krug, T. Schober, T. Springer, Solid State Ionics, 81 (1995) 111.

18. T. Schober, J. Friedrich, Solid State Ionics, 125 (1999) 319.

19. T.Tsuji, T. Nagano, Solid State Ionics, 136-137 (2000) 179.

20. T. Scherban, A. S. Nowick, Solid State Ionics, 35 (1989) 189.

21. N. Bonanos, B. Ellis, M. N. Mahmood, Solid State Ionics, 44 (1991) 305.

22. H. Iwahara, Y. Asakura, K. Katahira, M. Tanaka, Solid State Ionics, 3-4 (2003) 164.

23. F. M. Krug, Doctoral Thesis, RWTH Aachen (1996).

24. K.D. Kreur, Th. Dippel, W. Meyer, J. Maier, Mat. Res. Soc. Symp. Proc., 293 (1993) 273.

25. G. G. Scherer, E. Killer, D. Grman, Int. J. Hydrogen Energy, 17 (1992) 115.

26. M. Popall, Xin Min Du, Electrochim. Acta, 40 (1995) 2305.

27. J. Wei, C. Stone, A. E. Steck, patent W095/08581 (March 30, 1995).

28. G. Alberti, M. Casciola, Solid State Ionics, 97 (1997) 177.

29. C. A. Linkous, Int. J. Hydrogen Energy, 18 (1993) 641.

30. M. Rehahn, A. D. Schluter, G. Wegner, Makromol. Chem., 191 (1990) 1991.

31. K.D. Kreuer, Th. Dippel, J. Maier, Proc. Electrochem. Soc., 95 (1995) 241.

32. J. Maier, J. Electrochem. Soc., 134 (1987) 1524.

33. A. Kawada, A. R. Mcghie, M. M. Labes, J. Chem. Phys., 52 (1970) 3121.

34. T. Norby, in: Defect Chemistry of Solids, eds. ∅. Johannesen, A. Anderson, Elsevier, Amsterdam, (1990), p. 101.

35. F. A. Kroger, The Chemistry of Imperfect Crystals; North Holland Publishing Co., Amsterdam, (1964).

36. T. Norby, Y. Larring, Concentration and Transport of Protons and Oxygen Defects in Oxides; T. Norby, Y. Larring, Ed., The Institute of Materials, Maney Publishing North America, Cambridge, (1996), pp 83-93.

37. H. Iwahara, H. Uchida, K. Morimoto, S. Hosogi, J. Appl. Electrochem., 19 (1989) 448.

38. H. Iwahara, Solid State Ionics, 52 (1992) 99.

39. H. Iwahara, T. Hibino, T. Sunano, J. Appl. Electrochem., 26 (1996) 829.

40. T. Yajima, H. Kazeoka, T. Yoga, H. Iwahara, Solid State Ionics, 47 (1991)271.

41. W. Munch, G. Seifert, K. D. Kreuer, J. Maier, J. Solid State Ionics, 86-88 (1996) 647.

42. W. Munch, G. Seifert, K. D. Kreuer, J. Maier, Solid State Ionics, 97 (1997) 39.

43. K. D. Kreuer, Annu. Rev. Mater. Res., 33 (2003) 333.

44. T. Norby, Presented at Solid State Ionics Proc. SSPC-11, Survey, England, (2003).

45. K. D. Kreuer, Solid State Ionics, 125 (1999) 285.

46. Y. Larring, T. Norby, Solid State Ionics, 77 (1995) 147.

47. K. D. Kreuer, T. Dippel, Y. Baikov, J. Maier, Solid State Ionics, 86-88 (1996) 613.

48. M. Pionke, T. Mono, W. Schweika, T. Springer, Solid State Ionics, 97 (1997) 497.

49. T. Matzke, U. Stimming, C. Karmonik, M. Soetramo, R. Hempelmann, F. Guthoff, Solid State Ionics, 86-88 (1996) 621.

50. R. Hempelmann, M. Soetramo, O. Hartmann, R. Wappling, Solid State Ionics, 107 (1998) 269.

51. K. D. Kreuer, W. Munch, U. Traub, J. Maier, Ber. Bursenges. Phys. Chem., 102 (1998) 552.

52. F. Shimojo, K. Hashino, H. Okazaki, J. Phys. Soc. Jpn, 66 (1997) 8.

53. W. Munch, K. Kreuer, S. Adams, G. Seifert, J. Maier, Phase Transitions, 68 (1999) 567.

54. P. Kofstad, in: Non-stoichiometry, Diffusion and Electrical Conductivity of Binary Metal Oxides, Wiley, New York, (1972).

55. C. Wagner, Ber. Bunsenges, Physik. Chem., 72 (7) (1968) 778.

56. A. S. Nowick, W-K. Lee, H. Jain, Solid State Ionics, 28-30 (1988) 89.

57. J. Bates, J. Wang, R. Perkins, Phys. Rev. B, 19 (1979) 4130.

58. A. Mitsui, M. Miyayama, H. Yanagida, Solid State Ionics, 22 (1987) 213.

59. M. Scholten, J. Schoonman, J. van Miltenburg, HAJ. Oonk, Solid State Ionics, 61 (1993) 83.

60. S. Wienstroer, H. Weimhofer, Solid State Ionics, 101-103 (1997) 1113.

61. K. Ryu, S. Haile, Solid State Ionics, 122 (1999) 355.

62. K. Katahira, Y. Konchi, T. Shimura, H. Iwahara, Solid State Ionics, 138 (2000) 98.

63. M. Scholten, J. Schoonman, J. van Miltenburg, EHP. Cordfunke, Thermochim. Acta, 268 (1995) 161.

64. M. Scholten, J. Schoonman, J. van Miltenburg, HAJ. Oonk, Proc. Electrochem. Soc., 93/94 (1993) 146.

65. C. Tanner, A.Virkar, J. Electrochem. Soc., 143 (1996) 1386.

66. K. D. Kreuer, E. Schonherr, J. Maeir, in Proc. 14th Ris Int. Symp. On Materials Science, F. Poulsen, J. Bentzen, T. Jacobson, E. Skou, M. Ostergard, Eds. Ris, (1993) p. 297.

67. K. Szot, M. Pawelezyk, J. Herion, Ch. Freiburg, J. Albers, R. Waser, J. Hulliger, J. Kwapulinski, J. Appl. Phys. A, (1992).

68. S. Shin, H. Huang, M. Ishigame, Solid State Ionics, 40-41 (1990) 910.

69. H. Iwahara, T. Esaka, H. Uchida, N. Maeda, Solid State Ionics, 3-4 (1981) 359.

70. M. H. Zhen, X. Chen, Solid State Ionics, 70-71 (1994) 595.

71. V. Agarwal, M. Liu, J. Mat. Sci., 32 (1997) 619.

72. S. L. Peschle, M.Cifticioglu, D. H. Doughty, J. A. Voight, in Proc. Mat. Res. Soc. Symp., San Francisco, April 1992, edited by M. J. Hampden-Smith, W. G. Klemperer and C. J. Brinker, Mat. Res. Soc., Pittsburg, PA, (1992) p. 101.

73. M. Toprak, Yu Zhang, M. Muhammed, Materials Letters, 4460 (2003) 1.

74. P. S. Nicholson, Proc. Inter. Symp., Vol 7, The Metallurgical Society of Canadian Institute of Mining and Metallurgy, Calgary, Canada, June 1998.

75. R. D. Carneim, P. F. Becher, C-H. Hsueh, and T. R. Armstrong, Oak Ridge National Laboratory, Annual report, Oak Ridge, February 2002.

76. Western Oregon University, Constructing Porbaix diagrams, October 2000, www.wou.edu/las/physi/chapter 412/porbaix.htm, 4/3/2004

77. Eugenii Katz, Contributions of Marcel Porbaix, February 2004, www.geocities.com/neveyaakov/electroscience/porbaix.html, 4/4/2004

78. William F. Coleman, Porbaix diagrams, February 2003, www.wellesley.edu/Chemistry/chem120/pour.html, 4/3/2004

79. Albert I. King, Biocompatibility-Corrosion, January 1999, www.ttb.eng.wayne.edu/~grimm/BME5370/lect14Out.html, 4/4/2004

80. A. O. Isenberg, Solid State Ionics, 3/4, 431 (1981).

81. N. Minh, J. Am. Ceram. Soc., 76, 563 (1993).

82. A. Negishi, K. Nozaki, T. Ozawa, Solid State Ionics, 3/4, (1981) 443.

83. G. Meng, P. Wang, Y. Gu, D. Peng, Solid State Ionics, 136-137 (2000) 209.

84. M. C. Cheung, H. L. W. Chan, Q. F. Zhou, C. L. Choy, Nanostructured Materials, 11-7 (1999) 837.

85. L. Hong, X. Chen, Z. Cao, J. Euro. Ceram Soc., 21 (2001) 2207.

86. L. D. Landau, B. G. Levich, Acta Physiochim, U.R.S.S., 17 (1942) 42.

87. Debra L. Kaiser, Joseph J. Ritter- National Institute of Standards and Technology, Ceramic Division,Gaithersburg, June 2003,

88. Yanovskaya M. Ilyinichna: Promising Research Abstract PRA-4128, Karpov Institute Physical Chemistry, Moscow, June 1997.

89. M. Mennig, A. Kalleder, T. Koch, S. Mohr, C. Fink-Straube, S. Heusing, B. Munro, P. Zapp, H. Schmidt, proc. 2nd ICCG, Saarbrücken (1998).

90. C. J. Brinker, A. J. Hurd, K. J. Ward in Ultrastructure Processing of Advanced Ceramics, eds. J. D. Mackenzie and D. R.Ulrich, Wiley, New York (1988) 223.

91. Swedish Ceramic Institute, Tape Casting, November 2003, www.keram.se/eng/pdf/tapecasting, 2/10/2004.

92. School of Industrial and Manufacturing Science, UK, Engineering Design Systems, www.cranfield.ac, 2/5/2004.

93. S.-J. Song, E. D. Wachsman, S. E. Dorris and U. Balachandran, Solid State Ionics, 149 (2002) 1.

94. S.-J. Song, E. D. Wachsman, S. E. Dorris and U. Balachandran, J. Electrochem. Soc., 150 (2003) A1484.

95. S.-J. Song, E. D. Wachsman, S. E. Dorris and U. Balachandran, J. Electrochem. Soc., 150 (2003) A790.

96. S.-J. Song, E. D. Wachsman, S. E. Dorris and U. Balachandran, Solid State Ionics, accepted.

97. S.-J. Song, E. D. Wachsman, and H.-S. Yoon, J. Electrochem Soc., submitted.

98. S.-J. Song, E. D. Wachsman, J. Rhodes, S. E. Dorris and U. Balachandran, Solid State Ionics, in press.

99. S.-J. Song, E. D. Wachsman, J. Rhodes, H.-Yoon, G. Zhang, S. E. Dorris and U. Balachandran, J. Amer. Ceram. Soc., submitted.

BIOGRAPHICAL SKETCH

I was born in Dhule, India. After completing my high school I went to Maharashtra Institute of Technology, Pune, and earned my bachelor's degree in polymer engineering in August 2001. I was a teaching assistant for a few months and then decided to attend graduate school to pursue my Master of Science degree in materials science and engineering at the University of Florida.